JOURNAL OF GEOPHYSICAL RESEARCH, VOL. 97, NO. B11, PAGES 15,151–15,170, OCTOBER 10, 1992

62893

Volatile and Trace Element Composition of Melt Inclusions From the Lower Bandelier Tuff: Implications for Magma Chamber Processes and Eruptive Style

NELIA W. DUNBAR

Geoscience Department, New Mexico Institute of Mining and Technology, Socorro

RICHARD L. HERVIG

Center for Solid State Science, Arizona State University, Tempe

The Lower Bandelier Tuff, erupted from the Valles Caldera at 1.51 Ma, is composed of a Plinian tephra and associated ignimbrite. Based on ion and electron microprobe analyses of melt inclusions (MI) in quartz, sanidine, and pyroxene phenocrysts, a strong volatile gradient was present in the upper portion of the magma chamber. In the 20 km³ of magma that produced the Plinian tephra, most H_2O and F contents of MI are between 4 to 5 wt % and 0.18 to 0.20 wt%, respectively, and between 3 to 4 wt % and 0.12 and 0.14 wt % in the first-deposited basal ignimbrite. Measurements of the H_2O and F contents of the 380 km³ of magma which produced the bulk of the ignimbrite are concentrated between 2 to 3 wt% and 0.05 to 0.14 wt % respectively. The invariance of H_2O (and possibly Cl and B) relative to F in the magma which formed the Plinian tephra suggests that this portion of the magma chamber was saturated with respect to an H_2O-rich vapor phase. The trace element composition of MI are varied, and overlap with composition of pumice lumps. A group of MI are rich in Ti, Sr, Ba and low in B, Cl, Rb, Y, Nb, and Th, and are compositionally similar to analyses of matrix glass from some ignimbrite pumice lumps. These represent the mixing of a second rhyolite into the base of the Lower Bandelier magma chamber. MI influenced by the second magma have not been found in Plinian samples, but occur in ignimbrite samples from base to top of the deposit. When these MI are removed from the data set, the remainder show strong linear correlations between Nb and Rb, Y, Zr, and Th. These correlations can be most easily explained by fractionation of approximately ~40% quartz and alkali feldspar (with trace amounts of chevkinite). MI from the Plinian tephra are similar to bulk Plinian pumice composition, suggesting that magmatic evolution was well-progressed at the time that the MI were trapped. However, fractional crystallization is difficult to reconcile with the observed distribution of some other elements, including H, B, Li, F and Cl. The enrichment of H_2O and F in the upper portion of the magma chamber, along with their lack of correlation with Nb, Rb, Zr, Y, and Th, suggest that these sets of elements were decoupled during magmatic evolution. The upward enrichment of H_2O and F must have occurred at a faster rate than other trace elements. The observed volatile gradient may have influenced the eruption dynamics of the magma, initially causing discrete layers of magma to be removed when the gradient was large, followed by chaotic eruption of the bulk of the ignimbrite when the gradient was small. Comparison with the Bishop Tuff eruption, however, suggests that the chaotic eruption style of the LBT may be related to vent geometry and conduit evolution, promoting high discharge rates, not differences in the absolute concentration of volatiles.

Rayleigh #

INTRODUCTION

Many silicic tuffs show evidence of compositional zonation in their parental magmas. Although there is some variation in the style of zonation, eruptive sequences generally begin with the most evolved magma, and proceed towards less-evolved material. The specific mechanism by which compositional gradients are generated is unclear; in some cases fractional crystallization may be important, but in other cases, a more complex differentiation mechanism may be responsible [*Hildreth*, 1981; *Miller and Mittlefehldt*, 1984]. Systematic zonation in silicic magmas has been documented for major and trace elements, temperature, crystal contents, and compositions, and has been inferred for dissolved volatile contents of the magma [e.g. *Hildreth*, 1981]. Few direct determinations of volatile gradients in melts have been made [*Sommer and Schramm*, 1983, *Anderson*, 1991; *Dunbar and Hervig*, 1992], but gradients have been inferred from the type and quantity of phenocrysts in a magma, and also from changes in eruptive style characteristic of large eruptions [*Hildreth*, 1981]. Some magmatic systems appear to have contained a continuous gradient [e.g., *Hildreth*, 1979], whereas others show evidence of distinct compositional layers which produce step-wise, rather than smooth, compositional variations within their eruptive products [e.g., *Bacon*, 1983].

The preeruptive volatile content of a magma, particularly the pre-eruptive H_2O in a rhyolitic melt, may exert strong control on some aspects of the eruptive style. A gradient in the pre-eruptive water content of a rhyolitic magma may influence the transition from eruption of Plinian tephras to the eruption of ignimbrites, although other factors, particularly vent diameter, probably also contribute [*Wilson et al.*, 1980]. Furthermore, a significant pre-eruptive volatile gradient in a magma results in a corresponding density gradient, which may influence the geometry of magma removal from the chamber, allowing discrete compositional layers to be either sequentially or simultaneously withdrawn [e.g., *Blake and Ivey*, 198[illegible]; *Spera et al.*, 1986]. In general, if all other parameters are equal, eruption of a magma with small density gradient may tap a number of stratigraphic layers simultaneously, whereas a strong density gradient in a melt may allow relatively thin stratigraphic horizons to be tapped sequentially [*Blake and Ivey*, 1986].

The Lower Bandelier Tuff (LBT), erupted from the Valles Caldera in northwest New Mexico, was derived from a large silicic magma chamber. The LBT eruption began as a pumice fall, but soon shifted to ignimbrite deposition. The LBT deposit

Copyright 1992 by the American Geophysical Union.

Paper number 92JB01340.
0148-0227/92/92JB-01340$05.00

3558

is not systematically compositionally zoned, but there are compositional variations between individual pumice lumps, suggesting that the LBT is the product of a compositionally heterogeneous, and perhaps zoned magma chamber [*Kuentz*, 1986]. The dynamics of this type of eruption must be significantly different from those which produce compositionally zoned deposits, and may be a function of the density and viscosity gradients in the magma chamber. *Kuentz* [1986] interpreted the chemical zonation as a result of fractional crystallization, and implied that a volatile gradient, and resultant density and viscosity gradient would have been present as well.

Our objective in this work was to determine the pre-eruptive volatile gradient that was present in the magma which produced the LBT, based on analysis of the H_2O, Cl, and F contents of melt inclusions (MI) in LBT phenocrysts. These measurements allow assessment of the relationship between eruptive style, volatile, and density gradients. A secondary objective was to measure the trace element contents of bulk pumice and MI in order to aid in interpretation of the pristine nature of the MI. The data show that there was a large gradient in the H_2O content (hence density) of the magma between an H_2O-saturated cap (containing ~5 wt % H_2O, represented by the Plinian eruption) and the body of the chamber (which contained about 2.5 wt % H_2O). This gradient developed early in the evolution of the chamber. The trace element analyses of the MI and bulk rocks show that after the water gradient evolved, the chamber underwent ~40% eutectic fractional crystallization and was then intruded by a second rhyolitic magma at some time prior to eruption. This work is part of a larger project, aimed at investigation of volatile contents, gradients and eruption dynamics in a number of explosive rhyolitic systems, including the Bishop Tuff [*Dunbar and Hervig*, 1992], and the 2 ka Taupo pumice eruption (Dunbar et al., 1989a and b; Dunbar, 1991).

GEOLOGICAL BACKGROUND

The Jemez volcanic field, best known for the Valles caldera and the Bandelier Tuff, is situated on the western edge of the north-south-trending Rio Grande rift, and lies at the intersection of the rift with the northeast-trending Jemez volcanic lineament [e.g., *Goff et al.*, 1989]. The Jemez volcanic field has been active for the last 13 Ma, and has produced a variety of volcanic rocks, culminating in the eruption of the two major ignimbrites sheets which form the Bandelier Tuff and two associated collapse features, the Valles and Toledo calderas. The Bandelier Tuff and associated calderas have been the focus of pioneering work on resurgent calderas and compositionally variable ignimbrites [*Smith et al.*, 1961; *Smith and Bailey*, 1966].

Eruptive History of the Bandelier Tuff

The first Jemez Volcanic field magmas that appear to be genetically related to the Bandelier Tuff are the 4 Ma San Diego Canyon ignimbrites [*Turbeville and Self*, 1988]. The volume of these poorly exposed rhyolites has been estimated at >5 km^3 [*Turbeville and Self*, 1988]. The San Diego Canyon ignimbrites are chemically similar to the Bandelier Tuff, although slightly more mafic, and were probably derived from the same magma chamber [*Self et al.*, 1986; *Turbeville and Self*, 1988]. *Goff et al.* [1989] concluded that the San Diego Canyon ignimbrites were extensive features, and may have been erupted from a small caldera located near the western margin of the present-day Valles Caldera.

The Bandelier Tuff consists of two Plinian-ignimbrite pairs, the Lower Bandelier Tuff (LBT) and the Upper Bandelier Tuff (UBT). These two tuffs, erupted at 1.51 and 1.14 Ma, respectively [*Spell et al.*, 1990], have eruptive volumes of 400 km^3 and 250 km^3 DRE (dense rock equivalent) respectively [*Self and Lipman*, 1990]. The LBT was erupted from the ring-fracture system of the Toledo caldera, which was approximately coincident with the present-day Valles Caldera [*Goff et al.*, 1989]. Between the eruption of the LBT and the UBT a sequence of domes and pyroclastic falls and flows called the Cerro Toledo rhyolites, were erupted in the vicinity of the Toledo Caldera [*Stix et al.*, 1988]. Some of these deposits are present today around the northern and southeastern rim of the Valles Caldera. The UBT was erupted from the Valles caldera, possibly from a central vent location, rather than from ring fractures [*Self et al.*, 1986]. The degree of welding in the LBT and UBT ignimbrite sheets is variable, and most of the tuff is unwelded to moderately welded [*Smith and Bailey*, 1966; *Kuentz*, 1986].

Chemical Composition and Mineralogy of the Bandelier Tuff

The LBT and UBT are high-silica rhyolites which were derived from chemically heterogeneous, and perhaps systematically zoned, magmas. Both of these magmas may have been initially derived from a parental dacitic magma body, and compositional heterogeneity within the rhyolitic magma may be the result of fractional crystallization [*Smith*, 1979; *Kuentz*, 1986; *Balsley*, 1988]. Both the LBT and the UBT contain up to 30% phenocrysts, dominantly quartz and sanidine plus subordinate to trace amounts of pyroxene, magnetite, apatite and chevkinite. Other phases found in the LBT are allanite and zircon, whereas the UBT contains biotite, hornblende and ilmenite [*Kuentz*, 1986; *Balsley*, 1988]. Some trace element trends in the UBT are inconsistent with fractional crystallization, and may be a result of contamination by a dacitic magma [*Balsley*, 1988]. The magmatic temperature of the Plinian phase of the LBT was ~700°C, and the ignimbrite-producing magma was certainly hotter [*Warshaw and Smith*, 1988].

Although there is no simple relation between stratigraphy and bulk chemistry in the LBT ignimbrite, analyses of individual pumice fragments within the ignimbrite indicate that the magma chamber was compositionally heterogeneous. The elements Zr, Rb, Y, Nb, Cs, Th, and U show strong positive correlations, and the Plinian tephra is uniformly richer in these elements [*Kuentz*, 1986]. Niobium, the element which *Kuentz* [1986] used as a reference component following *Smith* [1979] ranges from 50 to 180 ppm among individual pumice lumps from the LBT ignimbrite and clusters around 185 ppm in the LBT Plinian samples. *Kuentz* [1986] suggested that a pre-eruptive chemical gradient was present in this magma, with the lowest Nb contents samples derived from deepest in the magma chamber, but that this gradient was destroyed by the eruptive process, and was therefore not recorded in the stratigraphy of the deposit.

Sommer and Schramm [1983] made measurements of H_2O contents in some MI from the LBT, and determined that magma which produced the Plinian tephra and ignimbrite contained ~5 and ~2 wt % H_2O respectively. However, since no trace element data were gathered for the glass in which the phenocrysts were found, there was no control on stratigraphic position in the pre-eruptive magma, and therefore the calculated volatile gradient would have large uncertainties.

The Cerro Toledo Rhyolites were erupted between the UBT and LBT and these are supposed to have tapped the liquids near the

top of the Bandelier magma chamber [*Stix et al.*, 1988]. They record the re-establishment of compositional zonation after the eruption of the LBT. This evolution occurred over about 0.37 Ma, and has been attributed to fractional crystallization of quartz, alkali feldspar, zircon and a light rare earth element phase [*Stix et al.*, 1988].

ANALYTICAL METHODS

Sampling and Sample Preparation

Bulk samples of Plinian tephra were taken at intervals through the exposed section, and individual pumice clasts were collected from the ignimbrite. Of these, three samples of the LBT Plinian, one sample from the UB Plinian, and nine samples from the LBT ignimbrite were selected for detailed study. Sample locations are given in Table 1. The three samples of Plinian tephra from the LBT deposit represent the base, center, and top of the tephra unit. Ignimbrite pumice samples were chosen based on freshness, availability of suitable melt inclusions (MI), and bulk chemical composition of the pumice. One half of each pumice clast was reserved for bulk chemical analysis; phenocrysts for MI analysis were separated from the other half. The portion of the pumice lump from which phenocrysts were separated was lightly crushed with a porcelain mortar and pestle, and sieved to 40 mesh. Phenocrysts of quartz, sanidine, and pyroxene were hand picked from the coarse fraction. In some cases, quartz was split from sanidine by heavy liquid separation (sodium metatungstate). The phenocrysts were then mounted in epoxy on 1-inch round glass slides, ground, and polished in diamond powder suspended in distilled water.

Electron Microprobe

Major elements and Cl were analyzed with a JEOL 8600 electron microprobe at Arizona State University. The error for Cl determinations was around ±100 ppm based on replicate analyses of reference material (glasses KE-12 and KN-18, from H. Sigurdsson; [see Devine et al., 1984]).

Ion Microprobe

Ion microprobe analyses were done in two stages. We first analysed MI with emphasis on H, Li, B, and F. Other trace elements were analysed with relatively low precision. Later, as we realized the interesting nature of the trace element data, we returned to selected MI and collected more precise trace element analyses. Analyses were made on a Cameca IMS 3f ion microprobe at Arizona State University. Analytical procedures follow *Hervig et al.* [1989]. A 1-2 nA mass-analyzed primary beam of $^{16}O^-$ ions was focussed to a spot 10-20 μm in diameter. Secondary ions were accelerated to +4500 eV and the transfer optics and field aperture were set to accept secondary ions into the mass spectrometer from a 20 μm circular area on the sample. After the secondary ion signal had stabilized (about 7 min) the sample voltage was ramped ±100 V from 4500, while the intensity of $^{30}Si^+$ was monitored. The sample voltage was returned to the centroid of the intensity versus sample potential curve to correct for the small amount of charging which occurred. The energy bandpass was fully open (130 eV) for early analyses, but in the later stages of this study we closed it to 40 eV. Molecular interferences were removed by collecting secondary ion intensities at high energies, which were achieved by offsetting the sample voltage -75 V from the centroid position for H, Li, B, F, P, Ti, Fe, Rb, Sr, Y, Zr, Nb, Cs, Ba, Ce and Th. In fact, there are no serious interferences on Li or B so it is not necessary to collect ion signals with an offset, but it was found that reproducibility of the analyses could be substantially improved by collecting all secondary ion intensities at the same sample voltage. There is no molecular interference on H, but the presence of a hydrogen background from the vacuum is very serious. *Hervig et al.* [1987] and *Hervig and Williams* [1988] found that the H background could be reduced by collecting data at an offset of a few volts. They concluded that the large number of secondary electrons generated during sputtering of oxides resulted in electron stimulated desorption (ESD) of surface hydrogen. This intense signal varied strongly with the secondary electron yield of the matrix. Because the energy spectrum of ESD ions is extremely narrow, a small voltage offset eliminated this source of background.

The secondary ion intensity for hydrogen was calibrated using experimentally hydrated rhyolitic glasses analysed by infrared spectroscopy (kindly provided by E. Stolper). Trace elements were calibrated against NBS 610, a sodium- and silica-rich glass containing nominally 500 ppm of 61 trace elements. Comparison of NBS-610 with several bulk-analyzed rhyolitic glasses indicated

TABLE 1. Locations for Lower Bandelier Tuff Samples

Sample	Quadrangle	Sample Location and Description
Plinian BB-096	White Rock	NW 1/4, NE 1/4 Sec. 21, T19N R7E; multiple pumice from 0.5 m above exposed base of ~7 m thick section of plinian tephra.
Plinian BB-094	White Rock	same as BB-096, multiple pumice from ~2 m above apparent top of section (top not well exposed)
Plinian BB-005	Puye	NE 1/4, SW 1/4 Sec. 32, T20N R7E; multiple pumice from top 0.5 m of 8 m thick Plinian section
Basal Ignimbrite BB-003	Puye	See BB-005, single pumice from 0.3 m above plinian-ignimbrite transition
Basal Ignimbrite BB-004	Puye	See BB-005, single pumice from 0.4 m above plinian-ignimbrite transition
Ignimbrite BB-021	White Rock	See BB-096, single pumice 25 m below top of ~40 m thick ignimbrite
Ignimbrite BB-045	Cañones	Polvadera land grant, ~1.5 miles south of town of Cañones, single pumice from 10 m below base of ~40 m thick ignimbrite section
Ignimbrite BB-037	Cañones	See BB-045, single pumice 4 m above base of ~40 m thick ignimbrite
Ignimbrite BB-014	White Rock	See BB-096, single pumice 15 m below top of ~40 m thick ignimbrite
Ignimbrite BB-027	White Rock	See BB-096, single pumice 24 m below top of ~40 m thick ignimbrite
Ignimbrite BB-030	White Rock	See BB-096, single pumice 5 m above base of ~40 m thick ignimbrite
Ignimbrite BB-057	Cañones	See BB-045, single pumice from near apparent top of ~40 m thick ignimbrite

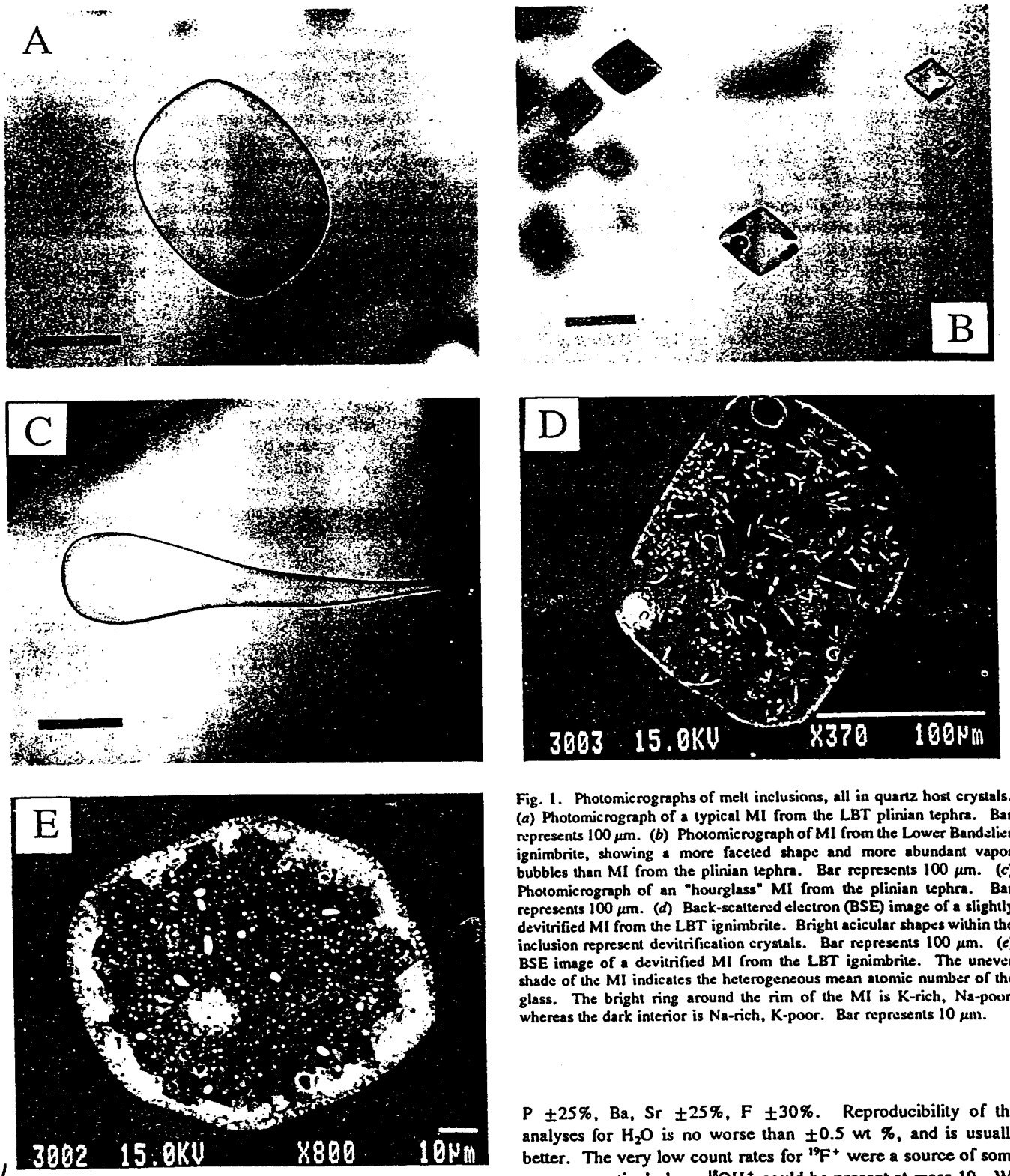

Fig. 1. Photomicrographs of melt inclusions, all in quartz host crystals. (*a*) Photomicrograph of a typical MI from the LBT plinian tephra. Bar represents 100 µm. (*b*) Photomicrograph of MI from the Lower Bandelier ignimbrite, showing a more faceted shape and more abundant vapor bubbles than MI from the plinian tephra. Bar represents 100 µm. (*c*) Photomicrograph of an "hourglass" MI from the plinian tephra. Bar represents 100 µm. (*d*) Back-scattered electron (BSE) image of a slightly devitrified MI from the LBT ignimbrite. Bright acicular shapes within the inclusion represent devitrification crystals. Bar represents 100 µm. (*e*) BSE image of a devitrified MI from the LBT ignimbrite. The uneven shade of the MI indicates the heterogeneous mean atomic number of the glass. The bright ring around the rim of the MI is K-rich, Na-poor, whereas the dark interior is Na-rich, K-poor. Bar represents 10 µm.

that the trace elements studied were within 10% of their nominal concentration. Exceptions are P and Ti, which are present in NBS-601 at levels of 350 and 590 ppm, respectively. Ion microprobe analyses reported in this paper the corrected value for NBS-610. Analyses for F used a combination of NBS 610 and KN-18, a comendite glass with 6400 ppm F. Observed reproducibility of secondary standards suggested that the precision of analyses are Li, B, Ti, Fe, Rb, Y, Zr, Nb, Ce and Th ±10%, P ±25%, Ba, Sr ±25%, F ±30%. Reproducibility of the analyses for H_2O is no worse than ±0.5 wt %, and is usually better. The very low count rates for $^{19}F^+$ were a source of some concern, particularly as $^{18}OH^+$ could be present at mass 19. We reanalyzed several MI from the Plinian tephra on the electron microprobe and obtained results within 200 ppm of the ion microprobe data.

Standards for Sodium ?

X Ray Fluorescence

X Ray fluorescence analyses were made of crushed pumice samples for Pb, Th, Rb, Sr, Y, Zr, and Nb. Analyses followed the procedure of *Norrish and Chappell* [1977], using a Rigaku 3062 instrument.

RESULTS

Petrography of Inclusions

MI in the LBT and associated Plinian samples (Figures 1*a* and 1*b*) are abundant in quartz, but also occur in sanidine and pyroxene. In the Plinian tephra, MI range from < 10 to 600 μm in diameter, with most between 50-200 μm. Bubbles in the MI from the Plinian tephra are rare, and where present are very small (< < 1% of inclusion volume). MI in crystals from the body of the LBT ignimbrite are smaller and less abundant than those from crystals in the Plinian tephra, and usually contain one or more bubbles. The glass:bubble ratio is variable for MI in the body of the LBT ignimbrite, but no vapor-dominated MI are present. Some ignimbrite MI contain many bubbles, but all are small. Total bubbles in ignimbrite MI generally represent <5% of MI volume. correct for this in H_2O analyses

Although MI in crystals from the Plinian tephra and completely unwelded portions of the ignimbrite are generally unbreached, some inclusions from ignimbrite samples are cracked, as has been described by *Skirius et al.* [1990]. Three main types of cracks have been observed, of which a single MI may be affected by none, some or all. First, some inclusions are surrounded by small, subtle radial cracks which are generally shorter in length than the diameter of the inclusion. These cracks tend to radiate from the most strongly curved areas, or "corners" of the inclusion walls. The second type of crack also radiates from the MI but is large scale and extends from the inclusion to the crystal edge. The third type of crack is also large and tends to extend to the edges of the crystal but does not appear to be directly related to inclusion, as the orientation relative to inclusions appears to be random. These cracks fracture the inclusion glass and therefore must have formed after the inclusion was relatively cool.

Several inclusion morphologies are seen in LBT crystals. Most MI are round to subrounded, and are evenly dispersed throughout the crystal. A second type of MI is found in quartz from the LBT Plinian and in some crystals from the LBT ignimbrite. The MI are long and thin, and are connected to the edge of the crystal (Figure 1*c*). These may be similar to the "hourglass inclusions" described by *Anderson* [1991] in the Bishop Tuff.

Many MI in crystals from the Plinian tephra are clear, and show no signs of devitrification or alteration. Optical and back-scattered electron imaging of MI suggests that there has been no post-entrapment crystallization. The crystal-melt contact is sharp, and no compositional gradient is apparent within the inclusions. Although many MI analysed from the LBT ignimbrite are pristine, some are incipiently to strongly devitrified. Devitrified MI are darker in color than pristine ones and some contain clots of crystals visible at low power magnification. Devitrification can also cause migration of Na and K within the glass, and this produces a mottled or zoned appearance in back-scatter imagery. Two stages of devitrification are shown in Figures 1*d* and 1*e*.

Major Elements

Major element composition of most MI were determined by electron microprobe to assess whether or not MI represent the magma which was present at the time that the crystals grew, or if any major alteration has affected the MI after trapping. Mean major element compositions of MI from the four Plinian samples from the LBT Plinian and UBT Plinian, and from the eight pumice lumps from the LBT ignimbrite which were analyzed as part of this study are shown in Table 2. Also shown in Table 2 are whole rock analyses for major elements in pumice samples from the LBT Plinian and UBT Plinian, and the mean whole rock major element composition from the LBT ignimbrite. The major element composition of pumice and MI are very similar within each of the eruptive units. The only possible exception to this close agreement is for Na_2O and K_2O in the LBT ignimbrite samples. The Na_2O and K_2O contents of pumice from the LBT ignimbrite are variable, and can be attributed to hydration and alteration of pumice [*Kuentz*, 1986], so MI compositions may actually be more representative of pre-eruptive magmatic liquids.

TABLE 2. Mean Major Element Composition of MI From the Plinian and Ignimbrite Phases of the Lower Bandelier Tuff, and a Plinian Tephra from the Upper Bandelier Tuff.

Sample Number	*n*	SiO_2, wt %	Al_2O_3, wt %	FeO, wt %	MnO, wt %	CaO, wt %	Na_2O, wt %	K_2O, wt %
Lower Bandelier Plinian Tephra Samples								
BB-096	41	77.5	12.1	1.3	0.1	0.3	4.2	4.4
BB-094	6	76.7	12.7	1.0	0.1	0.3	4.6	4.4
BB-005	11	77.2	12.0	1.3	0.1	0.3	4.4	4.4
Pumice*		77.1	12.2	1.2	0.1	0.3	4.3	4.4
Lower Bandelier Ignimbrite Samples								
BB-003	19	77.1	12.1	1.2	0.1	0.3	4.6	4.5
BB-004	20	77.2	12.3	1.0	0.1	0.2	4.6	4.4
BB-045	28	76.9	12.3	1.2	0.1	0.2	4.9	4.3
BB-037	25	77.2	11.9	1.2	0.1	0.3	4.5	4.6
BB-014	18	77.1	12.2	1.2	0.1	0.2	4.6	4.4
BB-027	22	77.2	12.2	1.2	0.1	0.2	4.3	4.5
BB-030	24	77.1	12.3	1.2	0.1	0.2	4.4	4.5
BB-057	8	77.5	11.8	1.2	0.1	0.3	4.6	4.4
Pumice*		77.3	12.0	1.0	0.1	0.3	4.0	5.0
Upper Bandelier Plinian Sample								
BB-092	21	76.1	12.6	1.1	0.1	0.3	3.8	5.6
Pumice†		76.2	12.3	1.3	0.1	1.3	3.4	5.4

All analyses are made by electron microprobe, and are recalculated water-free. The plinian samples are listed in stratigraphic order, and the ignimbrite samples are listed in order of inferred depth in the magma chamber. The n represents the number of analyses made of each sample.

*. Mean pumice composition from *Kuentz* [1986].

†. Mean pumice composition from *Balsley* [1988].

Post-entrapment crystallization apparently did not affect MI in the Bandelier Tuff. The composition of MI does not appear to be affected by the type of host crystal: analyses of MI in quartz, feldspar and pyroxene phenocrysts are indistinguishable, whereas if even a small degree of single-phase postentrapment crystallization had taken place the compositions would be systematically different [*Watson*, 1976]. Also, stepwise analyses across MI indicate that they are homogeneous.

Volatile Components

Over 150 analyses of H_2O, Cl, and F were made of MI from the Bandelier Tuff (Tables 3 and 4). Each value in Tables 3 and 4 represents from 1 to 3 analyses of a single MI. Most MI in Plinian tephras contain between 4 to 5.5 wt % H_2O and 0.2 to 0.3 wt % F (Table 3). In the LBT ignimbrite, MI in first-deposited, basal samples contain between 3 to 4 wt % H_2O and 0.1 to 0.2 wt % F, and those from the body of the ignimbrite contain approximately 2 to 3 wt % H_2O and 0.05 to 0.15 wt % F. Histograms of the H_2O and F contents of all analyzed samples, and of the H_2O contents of MI from individual ignimbrite samples

TABLE 3. Volatile and Trace Element Compositions of Melt Inclusions From the Upper and Lower Bandelier Plinian Tephras

Xtal	n	H_2O, wt %	Cl, wt %	F, wt %	Li	B	P	Ti	Rb	Sr	Y	Zr	Nb	Ba	Ce	Th	MI Color*	Mi Condition†
Base of plinian(BB-096)																		
fsp1	2	5.7	0.23	0.24	11	18		299	367		100						cl	v
qtz1	2	4.2	0.24	0.26	160	32											cl	v
qtz2	1	4.7	0.21	0.21	122	25											cl	v
qtz2	1	5.6	0.18	0.34	122	24											cl	v
qtz2	1	6.0	0.19	0.30	203	36											cl	v
qtz3	1	5.9		0.34	32	38											cl	v
qtz4	1	5.4	0.22	0.31	17	28	92	320	358	0.0104		250	206	5	72	42	cl	v
qtz4	1	4.4	0.25	0.27	28	23	132	252	381	1.9103		269	222	3	77	31	cl	v
qtz5	1	4.5	0.25	0.28	23	19	116	296	354	0	97	261	206	2	75	34	cl	v
qtz6	2	4.6	0.23	0.34	32	33											cl	v
qtz6	1	5.0	0.23	0.32	79	25	104	242	361	0.5	88	291	226	1	89	44	cl	v
qtz7	1	4.8	0.23	0.36	80	35											cl	v
qtz8	1	5.6		0.30	151	11	105	302	355	1.4	95	268	199	3	53	26	cl	v
mean		5.1	0.22	0.30	81	27	110	319	363	1.0	98	268	212	3	73	35		
Near top of plinian (BB-094)																		
qtz1	1	4.5		0.21	58	32											cl	v
qtz1	1	5.0	0.23	0.19	68	32											cl	v
qtz2	1	5.1		0.22	114	32											cl	v
qtz2	1	4.1	0.24	0.26	60	32											cl	v
qtz3	1	7.4		0.24	17	32											cl	v
qtz3	1	6.7		0.23	153	43											cl	v
mean		5.5	0.24	0.23	78	32												
Top of plinian (BB-005)																		
pyx1	2	5.6	0.21	0.15	12	17	86	274	337	0.6	117	260	189	3	102	36	cl	v
pyx1	2	3.9	0.18	0.15	82	11	70	346	296	0.3	72	192	137	3	83	25	cl	v
fsp1	2	4.0		0.21	83	17	81	306	320	4.9	86	223	174	5	69	32	cl	v
fsp2	1	4.1		0.16	101	16	58	329	278	0.4	95	228	184	3	80	34	cl	v
fsp3	1	4.1		0.11	59	24											cl	v
qtz1	2	4.0	0.21	0.17	84	21	53	303	338	0.1	97	246	198	3	75	41	cl	v
qtz2	1	4.7	0.22	0.18	189	35											cl	v
qtz3	1	3.1	0.20	0.22	47	23											cl	v
qtz4	1	4.0		0.23	76	23											cl	v
fsp4	1	4.9		0.10	48	6	70	542	283	1.1	89	235	174	5	64	28	cl	v
mean		4.2	0.20	0.17	78	19	69	350	309	1.2	92	231	176	4	79	33		
Upper Bandelier plinian (BB-092)																		
qtz1	1	5.9	0.33	0.28	112	35											cl	v
qtz1	2	4.5	0.29	0.23	59	32											cl	v
qtz1	1	3.9		0.22	91	26											cl	v
qtz1	1	3.5	0.34	0.29	124	32											cl	v
qtz1	1	4.2		0.27	58	32											cl	v
qtz2	3	4.1		0.22	37	29											cl	v
qtz2	1	4.3		0.25	65	32											cl	v
mean		4.3	0.32	0.25	78	32												

All elements were analyzed by ion microprobe with the exception of Cl, which was analyzed by electron microprobe. Each data set represents one or more analyses of a single MI. "Xtal" represents the crystal type and crystal number in which analyzed MI were located, and *n* represents the number of analyses made within each MI. Analytical errors are discussed in the text.

* Color of MI glass: cl, colorless.

† Condition of MI glass: v, vitreous.

are shown in Figures 2 and 3. The scatter for most multiple analyses of a single MI is low (~ ±0.2 wt %), the scatter for multiple MI within a single crystal is higher (Table 3 and 4), and the greatest scatter is found for analyses of MI in different crystals within the same sample (Table 3 and 4). As will be discussed later, although some of this variability is certainly real, some may be due to the sensitivity of ion probe analyses to the surface geometry of the sample. Surface geometry would tend to be most consistent within a single MI, and most variable between multiple crystals. Chlorine content of MI in the LBT Plinian are between 0.20 and 0.25 wt %, whereas in the Upper Bandelier (UB) Plinian samples Cl ranges from 0.29 to 0.34 wt %. Most MI in the LBT ignimbrite cluster between 0.17 and 0.23 wt % Cl. However, there is a set of MI, particularly noticeable in samples BB-014, BB-027, and BB-030 which contain between 0.10 and 0.14 wt. Cl.

Some severely devitrified MI were analyzed by ion microprobe and were found to be enriched in H_2O (up to 8 wt % H_2O for MI from the ignimbrite), possibly because H_2O becomes enriched in the residual glass as devitrification proceeds. These MI were only analyzed in order to see how devitrification affected the H_2O content, and are not included in the data set presented here.

TABLE 4. Volatile and Trace Element Compositions of Melt Inclusions From the Lower Bandelier Ignimbrite

Xtal	n	H_2O, wt %	Cl, wt %	F, wt %	Li	B	P	Ti	Rb	Sr	Y	Zr	Nb	Ba	Ce	Th	MI Color*	Mi Condition†
Basal ignimbrite (BB-003)																		
	2	4.1	0.14	0.17	55	14											cl	v
	2	2.5	0.15	0.13	25	15											lt br	v
qtz2	2	3.9	0.18	0.14	62	16											lt br	v
qtz3	1	3.2	0.15	0.12	58	12											cl	v
qtz4	1	4.3	0.23	0.11	44	21											cl	v
qtz5	1	4.2	0.17	0.14	108	25											cl	v
qtz6	3	3.5	0.18	0.16	41	12											lt br	v
qtz6	1	3.6	0.15	0.19	38	13											cl	v
qtz7	1	4.0	0.14	0.12	63	11											cl	v
fsp1	1	3.5	0.19	0.13	124	22											cl	v
qtz8	2	3.2	0.22	0.13	56	25											lt br	v
fsp2	1	2.2		0.13	22	12											cl	v
mean		3.5	0.17	0.14	58	16												
Basal ignimbrite (BB-004)																		
qtz1	1	4.0	0.21	0.11	124	15	343	257	326	1.2	90	266	184	4	82	38	lt br	v
qtz1	1	3.8	0.22	0.12	33	22	276	267	326	0.8	87	214	169	2	63	27	lt br	v
qtz2	1	4.1	0.24	0.13	43	13	258	284	335	0.8	88	235	172	4	66	35	cl	v
qtz3	1	4.6	0.18	0.15	46	16	255	291	225	0.8	88	281	178	6	86	33	cl	v
qtz3	1	3.8		0.09	48	11	203	382	276	1.1	56	167	91	6	76	16	cl	v
qtz3	1	4.1	0.21	0.13	50	17	232	296	284	0.5	90	280	167	3	73	28	cl	v
qtz4	1	5.2	0.20	0.12	33	8	162	352	225	0.7	48	162	91	3	69	21	cl	v
qtz4	1	5.5	0.21	0.10	30	11	204	263	335	0.0	71						cl	v
qtz4	1	4.6			152	21	201	261	365	0.1	70	213	173	2	58	29	cl	v
qtz4	1	5.0			150	21	196	238	358	0.8	72	182	148	1	50	27	cl	v
qtz5	1	3.3		0.22	73	11	235	382	212	0.5	33	164	89	3	70	11	cl	v
qtz6	1	5.2		0.19	127	23	231	295	351	0.4	78	205	180	5	53	19	cl	v
qtz7	1	4.1			19	15											cl	v
qtz8	1	4.5		0.12	88	28											cl	v
mean		4.4	0.21	0.13	73	17	233	301	302	0.6	73	215	149	3	68	26		
Ignimbrite Nb=161 (BB-021)																		
fsp1	2	1.8		0.05	100	33											cl	v
qtz1	2	2.2		0.03	48	32	172	215	314	0.3	90	214	155	9	62	19	dk br	v
fsp2	1	2.7		0.04	92	34											cl	v
tz2	2			0.10	59	34	115	216	329	0.3	85	208	165	6	68	24	lt br	v
qtz3	2	2.6		0.18	79	30	102	378	300	0.5	73	216	142	8	49	19	cl	v
qtz4	1	2.4		0.07	92	19											cl	v
qtz4	1	3.1		0.09	64	32											cl	v
qtz5	1	2.1		0.23	63	35	100	236	397	1.8	100	256	202	10	77	38	cl	sl dev
qtz6	1	2.4		0.04	52	30	88	271	370	0.5	73	216	140	8	49	19	lt br	v
fsp2	1	3.5		0.05			137	195	508	0.4	68	204	188	6	66	33	cl	v
mean		2.4		0.09	72	31	115	263	342	0.7	84	222	161	8	61	24		
Ignimbrite Nb=142 (BB-045)																		
qtz1	3	2.4	0.23	0.16	80	21	90	299	322	1.1	103	269	199	4	82	38	cl	v
qtz2	2	2.8	0.19	0.17	127	30											lt br	sl dev
qtz3	1	2.8	0.17	0.14	68	31											br	sl dev
qtz4	1	2.4	0.24	0.09	89	23	105	282	289	0.4	99	231	184	1	76	26	cl	v
qtz5	2	2.3	0.20	0.10	94	6	195	298	285	0.5	87	198	140	2	77	20	cl	v
qtz6	2	2.2	0.26	0.16	116	25	114	275	333	0.4	94	253	188	1	83	36	cl	v
qtz7	1	2.1	0.18	0.11	108	21											cl	v
qtz8	2	1.9	0.24	0.19	141	23	100	238	324	0.5	97	251	190	3	78	35	lt br	sl dev
qtz9	1	2.3	0.20	0.17	112	17	108	321	271	0.7	83	208	146	3	93	29	lt br	v
qtz10	1	1.9	0.24	0.10	32	23	387	285	299	0.7	83	235	196	3	71	31	cl	v
qtz11	1	2.4	0.20	0.08	81	17	214	315	270	0.6	82	208	155	3	86	30	cl	v
qtz12	1	2.3	0.18	0.09	107	17	187	316	282	0.6	83	209	145	1	87	27	cl	v
mean		2.3	0.21	0.13	96	21	167	309	297	0.6	90	229	171	2	81	30		
Ignimbrite Nb=140 (BB-037)																		
qtz1	1	2.7	0.21	0.12	64	32	76	351	341	1.1	87	226	175	5	67	34	cl	v
qtz2	1	3.0	0.22	0.12	83	35	66	328	352	0.7	93	229	159	2	78	36	lt br	v
qtz3	1	2.4	0.22	0.16	87	26	82	338	289	0.8	81	185	139	9	66	26	cl	v
qtz3	2	4.4	0.17	0.14	201	34	91	307	338	1.4	93	248	196	3	75	31	lt br	v
qtz4	1	2.7	0.15	0.16	209	31	63	297	335	0.5	85	213	148	2	63	25	lt br	v
qtz5	2	2.8	0.24	0.12	94	36	43	316	294	0.3	92	225	188	2	72	29	cl	v
qtz5	1	2.0	0.20	0.08	102	21	154	310	253	2.6	78	184	154	3	78	23	cl	v
qtz6	1	2.7	0.23	0.12	77	35	84	330	346	0.6	92	254	199	5	73	27	cl	v
qtz6	1	3.0	0.23	0.16	104	32	60	318	285	0.5	88	220	197	3	72	28	cl	v
qtz7	2	3.0	0.21	0.12	78	28											cl	v
qtz7	1	3.6	0.21	0.13	117	20	59	316	293	0.5	86	192	148	4	72	21	cl	v
qtz8	2	3.4	0.21	0.16	93	28	61	335	283	1.4	92	200	158	3	79	28	lt br	v
qtz9	1	3.5	0.15	0.13	247	34											lt br	v
mean		3.0	0.20	0.20	120	30	77	302	302	1.0	87	214	170	4	72	27		

TABLE 4 (continued)

Xtal	n	H_2O, wt %	Cl, wt %	F, wt %	Li	B	P	Ti	Rb	Sr	Y	Zr	Nb	Ba	Ce	Th	MI Color*	Mi Condition†
								Ignimbrite Nb=74 (BB-014)										
qtz1	1	1.9	0.13	0.04	51	17											cl	v
qtz1	1	1.8	0.19	0.01	49	32											cl	v
qtz2	1	2.0	0.21	0.04	64	31											cl	v
qtz3	1	2.2	0.17	0.05	50	15											br	v
qtz3	1	2.2	0.22	0.11	48	29											lt br	v
qtz4	1	2.0	0.13	0.05	57	12											lt br	v
qtz5	1		0.23	0.07	45	33											cl	v
qtz6	1	2.4	0.22	0.06	58	33											lt br	v
mean		2.1	0.19	0.05	53	25												
								Ignimbrite Nb=53 (BB-027)										
qtz1	1	2.3	0.21	0.06	15	83											br	v
qtz1	1	2.1	0.21	0.07	46	29											br	v
qtz2	1	2.0	0.21	0.07	43	17	141	273	227	1.2	81	274	162	5	67	24	br	v
qtz3	1	1.4	0.13	0.06	35	5	88	552	154	1.3	34	200	59	10	79	13	cl	v
qtz4	1	0.7	0.13	0.06	41	22											dk br	v
qtz5	3	1.4	0.15	0.07	47	10	156	255	281	0.9	64	252	122	5	61	22	dk br	v
qtz6	2	1.8	0.18	0.12	31	10	84	314	284	2.0	60	175	142	6	55	18	br	v
qtz6	1	2.3	0.19	0.10	46	19	73	320	292	2.0	86	212	161	5	67	38	cl	v
qtz6	1	2.9		0.08	47	7	61	240	294	0.6	80	245	151	1	75	33	cl	v
qtz7	1	2.3	0.10	0.04	38	10	179	558	187	2.8	30	210	60	11	84	13	cl	v
qtz7	1	1.0	0.25	0.06	41	32											cl	v
qtz8	1	1.8	0.12	0.09	42	10											cl	v
mean		1.9	0.17	0.07	39	22	100	414	255	1.3	68	226	133	5	67	25		
								Ignimbrite Nb=52 (BB-030)										
qtz1	1	4.1	0.17		72	6	105	307	196	0.8	42	130	96	4	38	12	cl	sl dev
qtz2	1	3.3	0.12	0.04	31	3	94	606	151	2.3	33	234	64	9	76	8	lt br	v
qtz3	1	1.9	0.12		50	5	103	593	120	1.2	33	193	58	8	70	9	cl	v
qtz4	1	3.0	0.22	0.03	45	19	107	242	226	1.6	83	245	168	5	58	21	cl	v
qtz5	1	1.3	0.11	0.07	66	4	107	618	118	0.8	28	180	50	5	66	8	lt br	v
qtz6	2	3.0	0.23		37	6	204	428	77	0.7		206	134	3	50	29	cl	sl dev
qtz7	1	2.3	0.11	0.08	61	5	110	597	115	1.3	29	188	54	8	68	8	dk br	v
qtz8	1	3.3	0.11	0.07	37	5	79	549	87	1.4	26	172	29	7	60	10	lt br	v
qtz9	1	3.2	0.23	0.05	21	2	89	246	299	0.5	68	226	145	2	53	25	cl	sl dev
qtz10	1	2.5	0.22	0.11	55	10	79	287	283	0.4	66	238	96	3	50	24	cl	v
qtz11	1	3.0		0.16	46	4	92	447	118	0.6	40	157	64	2	52	12	cl	v
qtz12	1	4.6		0.11	38	3	125	577	126	1.0	24	160	48	8	48	12	cl	v
qtz13	1	2.3		0.22	30	18	73	261	249	1.9	68	210	143	4	46	23	cl	v
qtz13	1	3.0		0.11	38	4	100	637	139	2.6	27	175	48	11	64	12	cl	v
mean		2.9	0.16	0.06	45	7	105	443	167	1.1	42	195	88	5	57	15		
								Top of ignimbrite (BB-057)										
qtz1	1	1.6	0.21	0.08	86	28											br	cl
qtz1	2	2.0	0.19	0.08	102	29											br	v
qtz2	2	2.2	0.23	0.15	87	35											lt br	v
qtz3	1	1.8		0.09	95	36											lt br	v
qtz3	1	2.2		0.15	82	24											lt br	v
qtz4	1	2.4	0.22	0.22	95	30											cl	v
mean		2.1	0.21	0.13	91	30												

All elements were analyzed by ion microprobe with the exception of Cl, which was analyzed by electron microprobe. Each data set represents one or more analyses of a single MI. "Xtal" represents the crystal type and crystal number in which analyzed MI were located, and *n* represents the number of analyses made within each MI. Analytical errors are discussed in the text.

* Color of MI glass: cl, colorless; lt br, light brown; br, brown; dk br, dark brown.

† Condition of MI glass: v, vitreous; sl d, slightly devitrified.

Trace Elements

Ion microprobe analyses of Li, B, P, Ti, Rb, Sr, Y, Zr, Nb, Ba, Ce, and Th for MI are listed in Tables 3 and 4. Whole rock analyses for Pb, Th, Rb, Sr, Y, Zr, and Nb in pumice lumps are given in Table 5. The new pumice analyses are within the range of compositions determined by *Kuentz* [1986]. MI show a similar compositional range as whole-pumice analyses. A number of trace elements in MI, including Nb, Rb, Zr, Y, and Th, covary and overlap with the range of bulk analyses (Figures 4*a* and 4*b*). MI analyzed from the Plinian tephra overlap with the most evolved ignimbrite MI compositions (Figures 4*a* and 4*b*, Figure 8*a*). MI compositions in the Plinian tephra are similar to the bulk composition (Figure 4*c*) whereas in some ignimbrite samples, a population of MI are enriched in the aforementioned elements with respect to the bulk composition of the pumice in which the MI were found (Figure 4*d*).

The analyses are most simply described as falling into two groups. The first group, the so-called "normal" LBT composition, includes MI from ignimbrite and Plinian pumice lumps which show Nb ranging from 120-230 ppm and Ti from 190-350 ppm (the "normal field", Figure 4*e*). The Plinian MI are distinguished by their high H_2O and F contents (described previously). The

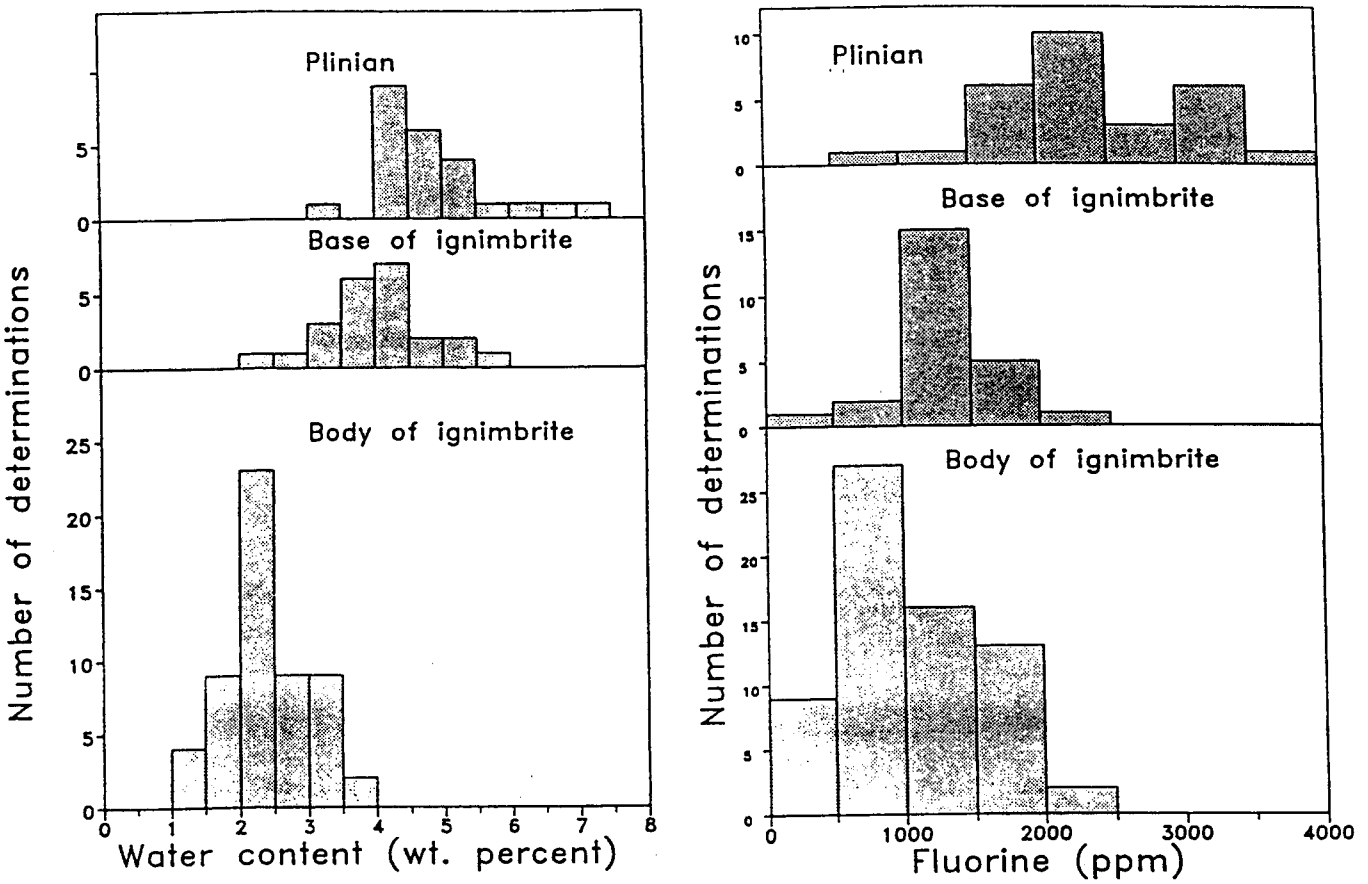

Fig. 2. Histogram of volatile contents of all MI from the LBT plinian and ignimbrite as analyzed by ion microprobe. (*a*) Histogram of H_2O. (*b*) Histogram of F.

second group consists of a suite of MI from ignimbrite samples 004, 014, 027, and 030 which are characterized by high titanium and low Nb (Nb from 30 to 100 ppm, and Ti from 350 to 637 ppm, the "high-Ti" group Figure 4*e*). The high-Ti MI are also richer (on average) in Sr and Ba but are poorer (on average) in Cl, Li, B, Rb, Y, Nb, and Th (Figures 4*e* and 4*f*). There is no statistically significant difference between the low- and high-Ti ignimbrite MI for P, Fe, and Ce.

The distinction between the high and low-Ti MI does not appear to be sharp when all data are considered (Figures 4*e* and 4*f*). However, when analyses from a single pumice lump are examined, the differences are more pronounced. This comparison is shown on Figure 5 (Ti versus Cl, Y, Ba, and Th) for sample 030, where bulk and microbeam data are compared. Whole rock analyses of the pumice lump are similar to the analyses of high-Ti MI and the single analysis of matrix glass. While on average there is a difference in the Li and F contents between high- and low-Ti MI, this difference does not show up on the scale of a pumice lump. Note that single quartz crystals in samples 030 and 004 contain a high- and a low-Ti MI. The relative positions of these MI within the crystal is difficult to ascertain because of cutting geometry.

The single pumice analyses by *Kuentz* [1986] and those made as part of this study also can be split into the same groups. Pumice analyses show distinctly high Zr in the high-Ti suite of samples. Kuentz analyzed several elements not studied here, and we note that Eu and Sc are enriched in the high-Ti samples while Ga, Sb, Cs, Ta, U, Zn, Hf, Sm, and heavier trivalent rare earth elements are depleted relative to low-Ti pumice. The analyses by *Kuentz* [1986] indicated that Plinian samples do not show a wide range of chemistry while ignimbrite samples can be quite variable. The ion probe data also show less variability in Plinian MI compositions. In general, analyses of ignimbrite pumice samples best match the MI containing the lowest Nb.

Step scans for Li, P, Ti, Rb, Sr, Ce, and Ba were made across three sanidine crystal from LBT ignimbrite sample BB-027 and four sanidine crystals from LBT ignimbrite sample BB-021 (Figure 6). In one of the crystals analyzed from BB-027, the core of the phenocryst contains low and constant abundances of Ba, Sr, Ti, and Ce, but these elements are enriched by factors of 5, ~1.5, 2 and 5 respectively, beginning about 400 μm from the rim of the crystal. Strontium, Ba, Fe (not shown), Ti and P increase sharply at about 200 μm from the crystal edge, but then tend to fall sharply again. Rubidium and Li are virtually constant from 200 to 700 μm (Figures 6*a* and 6*b*). Barium, Sr, Ti, and Ce are strongly correlated in this sanidine. The two other sandine crystals from BB-027 showed similar correlations between Ba, Ti, Sr, and Ce near the crystal margins but absolute concentrations were lower.

Three of the crystals from BB-021 are homogeneous with respect to Rb (Figure 6*d*), with concentrations of ~115 ppm. One of the three crystals contains a MI with 300 ppm Rb (scan 3). The resulting calculated partition coefficient (0.3) is consistent with other measurements [e.g. review in *Nash and Crecraft*, 1985; *Kovalenko et al.*, 1988]. Li decreases by 30-50% at the rims of sanidines. Two step scans at right angles were made across a fourth crystal from sample 021 contains about 50 ppm Rb. In the long direction of the sanidine, the Rb increased from ~50 ppm at the core to 90 ppm at the rim, while in the other direction the Rb remained uniformly low.

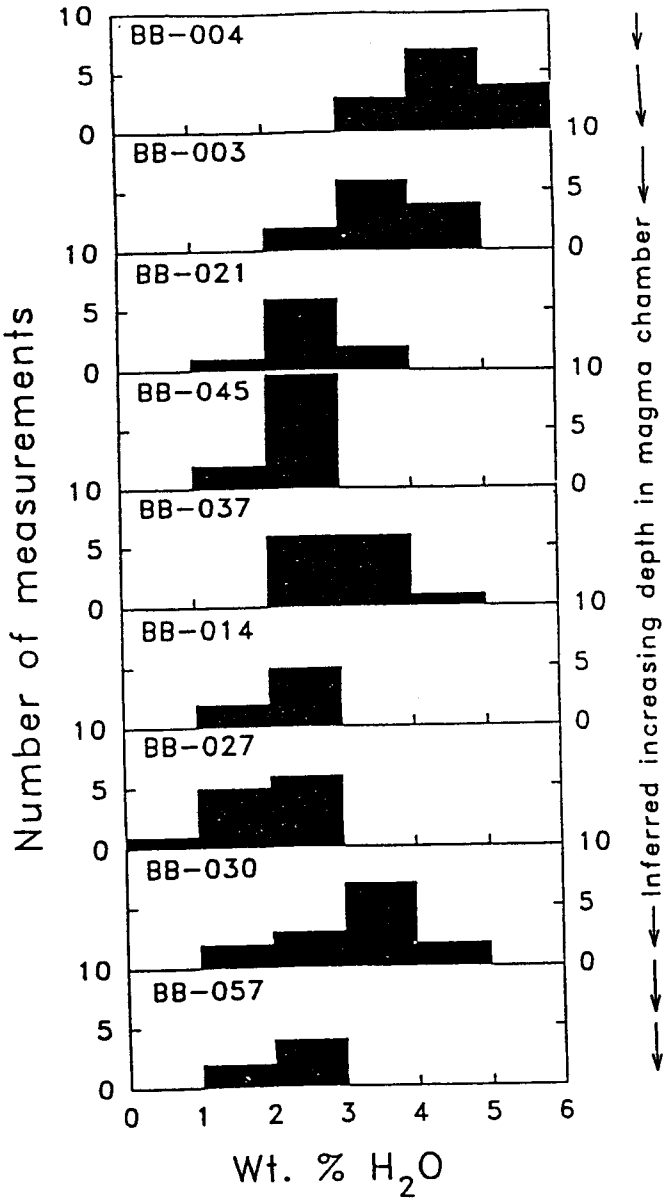

Fig. 3. Histogram of the H_2O content of MI from individual LBT ignimbrite samples. The samples are arranged in order of inferred depth in the magma chamber. The "basal ignimbrite" samples are located based on stratigraphic position in the deposit. The samples from the body of the ignimbrite are arranged in order of decreasing whole pumice Nb content. Sample BB-057 was too small for bulk trace element determination.

TABLE 5. Trace Element Compositions of Bulk Pumice and Matrix Glass From the Body of the Lower Bandelier Ignimbrite

Sample Number	Pb, ppm	Th, ppm	Rb, ppm	Sr, ppm	Y, ppm	Zr, ppm	Nb, ppm
Bulk Pumice							
Basal ignimbrite							
BB-002	30	29	211	9	68	173	100
BB-003	28	25	194	12	61	174	90
BB-004	27	25	211	9	60	170	86
Body of ignimbrite							
BB-014	13	22	162	7	52	182	74
BB-021	14	43	307	3	105	223	161
BB-027	15	17	117	6	37	215	53
BB-030	17	13	114	5	38	201	52
BB-037	36	39	284	12	96	201	140
BB-045	31	40	285	15	96	206	142
Matrix Glass							
BB-027		14	110	4	25	184	55
BB-037		32	310	2	86	217	166

Whole pumice analyses by Xray fluorescence analysis, and matrix glass analyzed by ion microprobe.

Are Melt Inclusions Representative of Preeruptive Melt?

Melt inclusions are small samples of magmatic liquid which are trapped in crystals during their growth [*Roedder*, 1984]. If unaltered, these MI can provide direct samples of preeruptive silicate. Any investigation of MI must involve detailed assessment of the quality of the inclusions in order to determine if alteration has taken place. A number of factors may cause MI compositions to deviate from true pre-eruptive magmatic liquid composition. For example, if a MI remains at near-magmatic temperature for an extended time, additional crystalline material may precipitate onto its interior wall. If a single crystalline phase, that of the host crystal, is deposited, the remaining glass becomes enriched or depleted in the elements which are respectively incompatible or compatible in this crystal [*Webster and Duffield*, 1990; *Watson*, 1976; *Anderson and Wright*, 1972]. If a eutectic assemblage were deposited, the residual glass might not be altered with respect to major elements, but the secondary crystals would not be optically continuous with the host crystal. Eutectic crystallization within a MI has not been observed in other magmatic systems. Based on the close agreement between the major element compositions of MI and matrix glass, and the lack of an optically discontinuous layer bounding the glass, MI in the Bandelier Tuff appear to be pristine. The slight negative crystal shape observed in some MI from the LBT ignimbrite may be a result of crystal annealing [*Anderson*, 1991].

Inclusion glass may become devitrified after entrapment, particularly if the MI remains at high temperature for an extended time. Devitrified MI can be recognized with petrography, major element analyses, and backscatter electron imaging, so analysis of these MI was avoided. Incipient devitrification can be more difficult to recognize in a MI but *Skirius et al.* [1990] suggest that incipient devitrification does not affect the volatile content of MI.

MI may trap non-representative magma. For example, if the crystal grew faster than a specific element could diffuse away from the crystal-melt interface, an envelope of anomalous melt around the crystal could result [*Bacon*, 1989]. This effect can be difficult to assess in MI because the diffusional process is complex, and may affect some elements more than others. For example, it is apparent from the variable trace element compositions of MI in a single pumice lump that MI may not be compositionally identical to the bulk melt+crystals from which they were trapped. However, the lack of correlation between the variable trace elements (Rb, Y, Nb, Cs, Ce, and Th) and volatile components suggests that the processes responsible for the trace element chemistry did not influence the volatile content.

Some MI contain bubbles that may have been trapped during crystal growth [*Belkin et al.*, 1985] or, may have evolved during cooling due to differential contraction of the host crystal and inclusion glass [*Roedder*, 1984]. Bubbles which evolve in MI may contain a vapor phase, but bubbles in MI from the LBT probably do not contain a significant amount of H_2O, due to their small size (<5% of total MI volume) and the high H_2O content of bulk glass.

Finally, it is possible that MI may lose H_2O, particularly if they are held at elevated temperatures for long periods of time. Ideally, MI for volatile analysis should have quenched rapidly, as the diffusion rate of water increases with temperature [*Karsten et al.*, 1982; *Hofmann*, 1980]. However, rapidly quenched samples of ignimbrites may be difficult to obtain. In some cases, MI appear to have degassed through "sub-micron capillaries" [*Bacon et al.*, 1992], or through large cracks in the host crystal [*Skirius et al*, 1990]. We attempted to avoid analysing MI which were penetratively cracked. Some host crystals contain small radial fractures around the included glass, but the volatile content of these slightly fractured MI does not appear significantly different than those from uncracked crystals. Some MI with anomalously low H_2O contents were disgarded because of the possibility of unobserved penetrative cracking. The volatile contents of MI which showed slight radial cracking were similar to those which appeared uncracked, as was also observed by *Skirius et al.* [1990]. However, *Skirius et al.* [1990] suggest that, in some slowly cooled

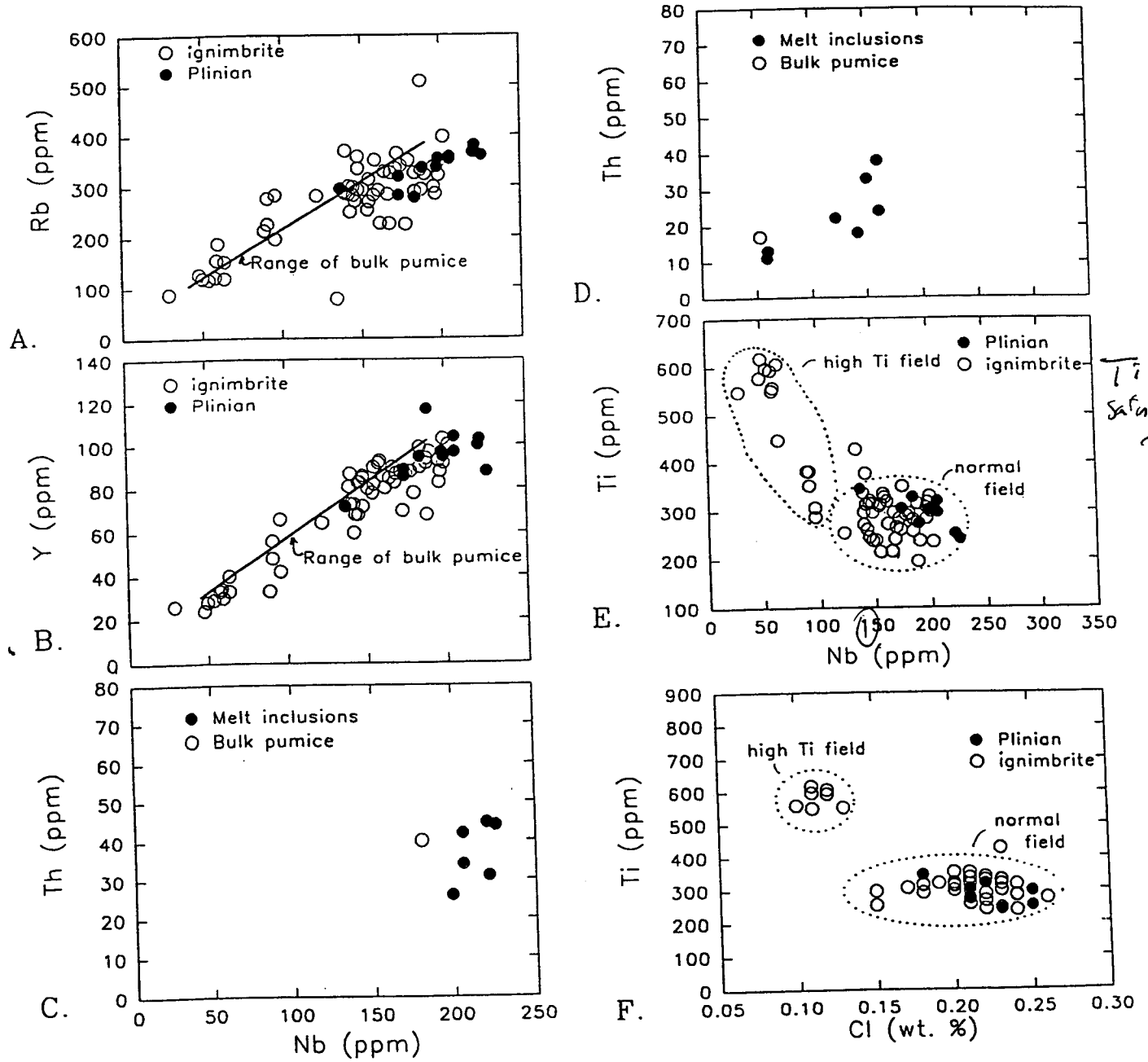

Fig. 4. Plots of trace element contents of MI from the LBT as analyzed by ion microprobe. Solid circles represent MI from the plinian tephra, and open circles are from the ignimbrite. (*a*) Nb versus Rb for all MI. The line on the figure represents the range of bulk samples as analyzed by *Kuentz* [1986]. (*b*) Nb versus Y for all MI. The line on the figure represents the range of bulk samples as analyzed by *Kuentz* [1986]. (*c*) Nb versus Th for MI from a single sample of LBT plinian tephra. The open circle represents bulk composition of plinian tephra as determined by Xray fluorescence by *Kuentz* [1986]. (*d*) Nb versus Th for MI from a single pumice lump (BB-027) from the LBT ignimbrite. The open circle represents the bulk composition of the pumice lump as determined by Xray fluorescence analysis. (*e*) Plot of Ti versus Nb for all MI from the LBT as analysed by ion microprobe. The outlined field represents the "high-Ti" composition MI; others are part of the "normal field." (*f*) Plot of Ti versus Cl for all MI from the LBT as analyzed by ion microprobe. The outlined field represents the "high-Ti" composition MI, all others are part of the "normal field."

ignimbrites, vitreous rhyolitic MI have been affected by cracking and that presumably the loss of volatiles allowed the MI to remain vitreous. They suggest that unaltered volatile contents can be most reliably determined by revitrifying devitrified MI. Therefore, we would like to acknowledge that some of the lower H_2O contents of MI may result from analysis of MI with undetected cracks, which have lost H_2O.

The process of diffusive hydrogen loss [*Qin and Anderson*, 1992] is difficult to address in a natural system, because the MI from the ignimbrite remained at high temperature for longer than those from the Plinian tephra and the relatively lower water contents measured could also result from expected from predicted volatile element zonation (higher volatile contents near the top of the chamber). We were able to collect one sample (BB-057) from the pumice-poor, completely nonwelded top of the LBT ignimbrite, which probably cooled rapidly compared to the body of the ignimbrite. The volatile contents of the MI from this sample were similar to other samples from the body of the ignimbrite.

Variations in the H_2O contents of LBT MI in a pumice lump tend to exceed our estimated analytical uncertainty of ± 0.5 wt %. The magnitude of variability appears to increase with the scale of observation, being lowest for multiple analyses of a single MI and highest for MI in different crystals. Some MI contain abnormally high water contents (e.g., Table 3, Figure 7*a*) which could be attributed to spurious individual analyses, but high values have also been observed in MI using other analytical techniques [e.g., *Skirius et al.*, 1990]. However, magma in a natural system is not necessarily homogeneous [e.g., *Oldenberg et al.*, 1989], and some of the variations observed are likely to be due to local inhomogeneity in the volatile concentrations in the magma

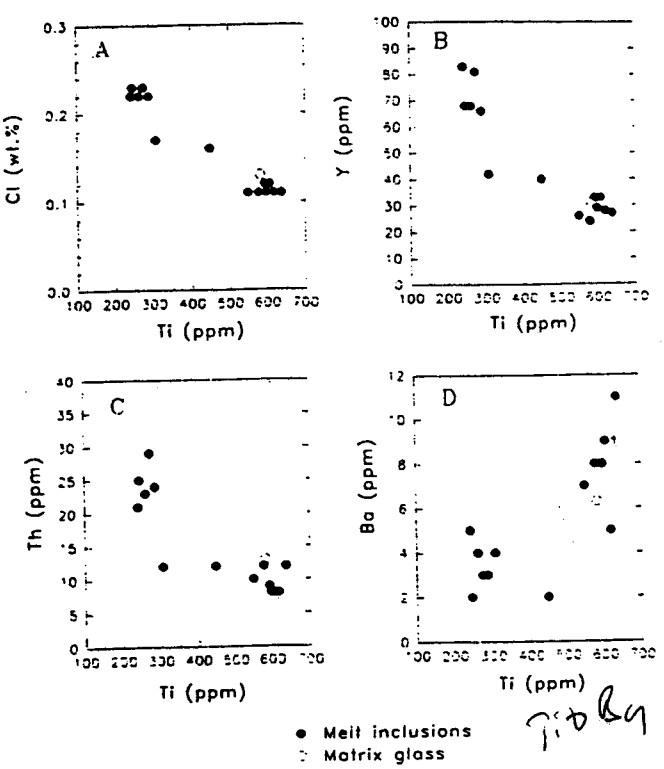

Fig. 5. Trace element compositions of MI from ignimbrite sample BB-030, emphasizing the high-Ti and normal composition MI. (*a*) Ti versus Cl; (b) Ti versus Y; (c) Ti versus Th; (d) Ti versus Ba. Solid circles represent MI analyses, and the open circles represent analyses of matrix glass.

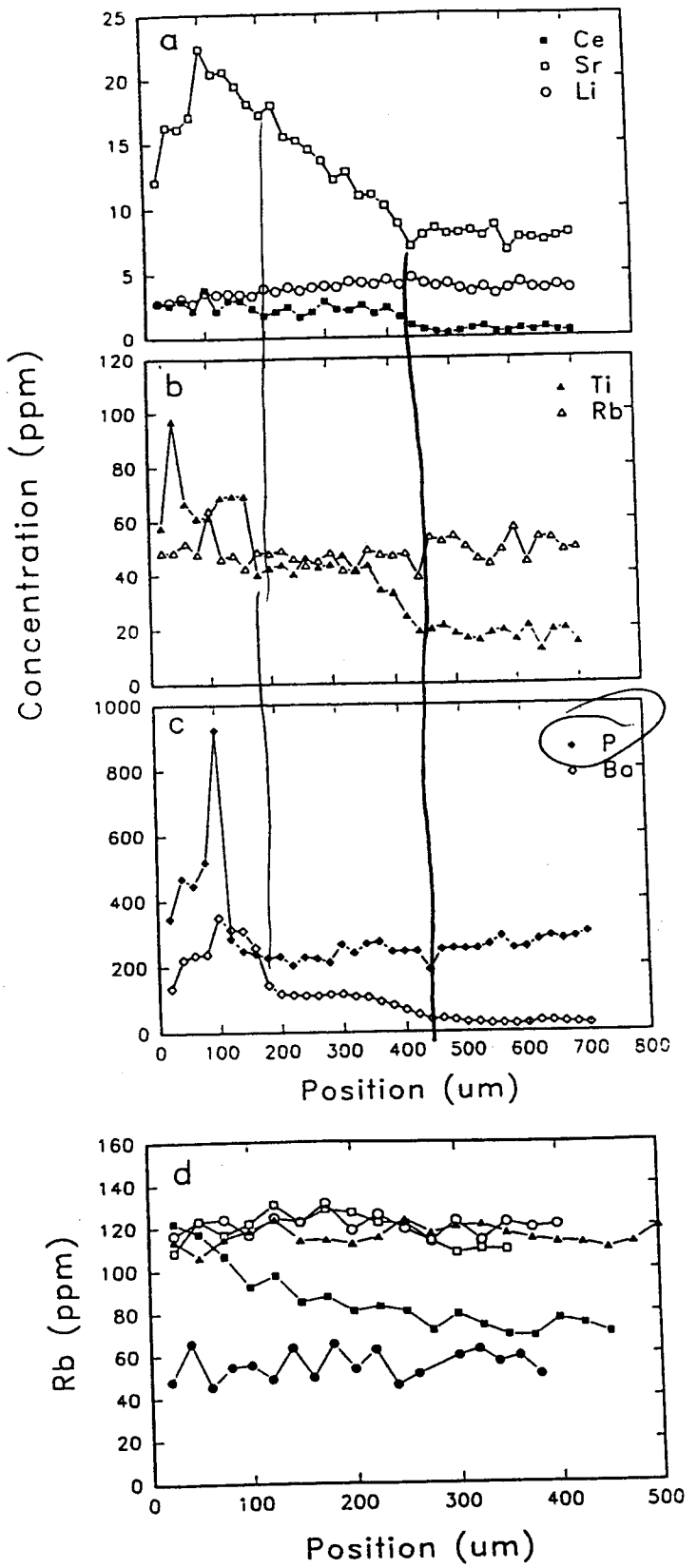

Fig. 6. Variations of trace elements with distance from the rim of sanidine crystals. The x-axis represents position in the crystal, with 0 as the edge. (*a*) BB-027, Sr and Ce are low and constant in the interior, but increase towards the crystal edge. (*b*) BB-027, Ti is similar to Sr and Ce, but Rb is nearly constant, at 45-50 ppm. (*c*) BB-027, P declines steadily edgewards to ~125 μm, where it increases dramatically, then declines. Ba behaves similarly to Ti, Ce, and Sr. (*d*) Four sanidine crystals from BB-021. Two different Rb compositions are indicated, and one crystal appears transitional between the two.

chamber. On a larger scale, pre- or syn-eruptive processes could also be important, including settling of crystals in a zoned magma chamber or small-scale mixing (on the scale of a single pumice lump) of magmas with distinct volatile contents at the time of eruption [*Blake and Campbell*, 1986; *Carrigan and Eichelberger*, 1990].

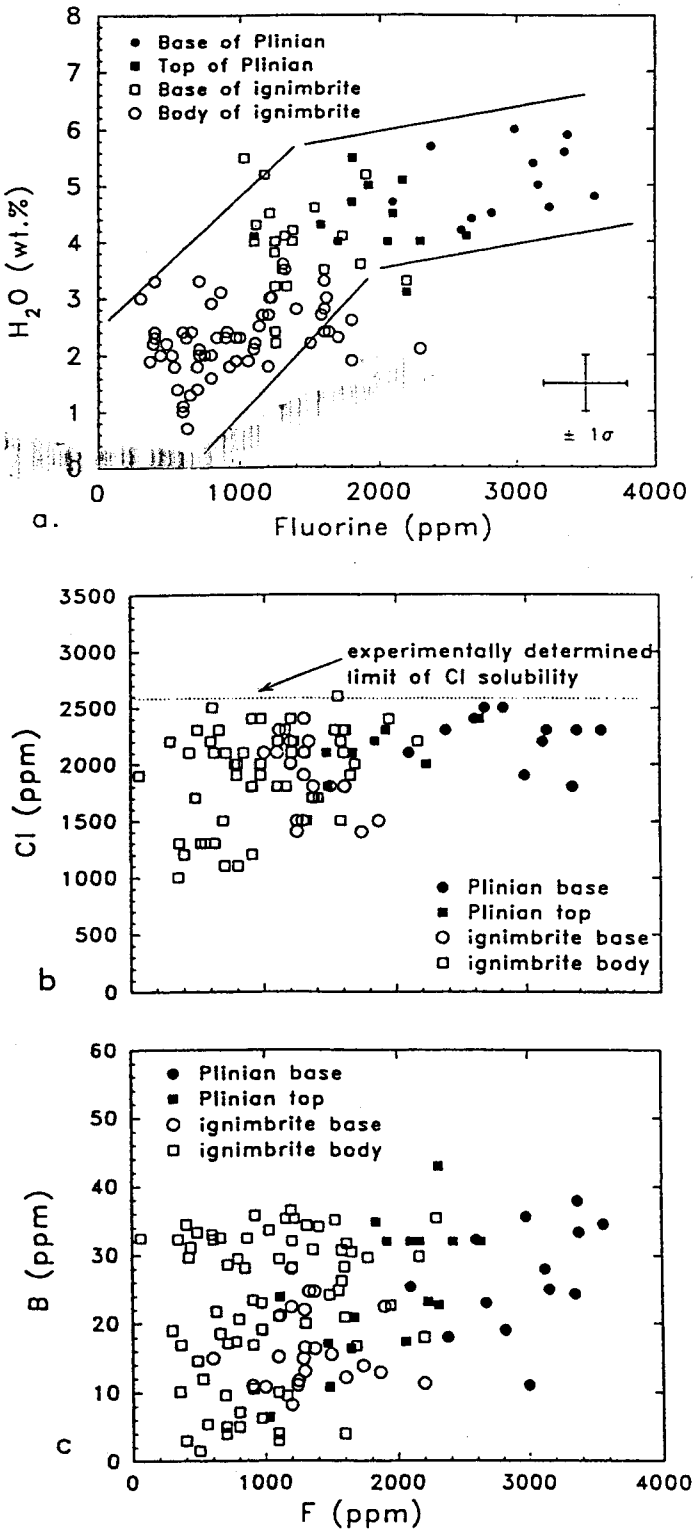

Fig. 7. Fluorine versus (*a*) H_2O, (*b*) Cl, and (*c*) B. The dotted line on Figure 7*b* shows the experimentally determined maximum Cl content of rhyolite in the presence of an H_2O-rich vapor phase [*Webster and Holloway*, 1988]. Precision of analysis for H_2O is ± 0.5 wt %, Cl ± 100 ppm, F ± 300 ppm and B ± 6 ppm.

DISCUSSION OF VOLATILE DISTRIBUTION

Volatile Distribution in the Lower Bandelier Magma

Our determinations show that a significant volatile gradient was present in the LBT magma chamber, with higher H_2O and F in the upper zone which produced the LBT Plinian as compared to that which formed the LBT ignimbrite (Tables 3 and 4; Figures 2 and 3). The greatest and most systematic amount of variation in preeruptive H_2O and F content appears to be in the magma which produced the Plinian tephra and the directly overlying ignimbrite, which we presume to represent the top of the magma chamber. The mean H_2O and F contents of these samples vary from 5.5 to 3.5 wt % and 3000 to 1200 ppm, respectively. The variation in volatile contents for this portion of the magma chamber appears to be stratigraphically preserved in the deposit, suggesting that, at least in this part of the eruption, sequentially deeper layers of the magma chamber were being removed. This eruptive style has also been suggested for the early stages of eruption based on field evidence [*Self and Lipman*, 1989]. Within the body of the ignimbrite, there is no systematic variability in the mean H_2O and F contents of individual samples (Table 4) with either stratigraphic position in the deposit, or with trace element concentration of the whole rock pumice sample. Although the samples from the basal ignimbrite are more enriched in H_2O and F than those from the body of the ignimbrite, there is no positive correlation between these two components in the body of the ignimbrite. Therefore, on a large scale, the H_2O and F contents of the >300 km^3 of the magma which produced the bulk of the ignimbrite appears to have been relatively uniform.

The abundance of MI in magmatic phenocrysts also provides indirect evidence of the volatile gradient in the LBT magma. We observe that quartz crystals in the LBT Plinian tephra contain abundant MI (estimated at up to 20% of the crystal volume), whereas MI abundance is lower in the basal ignimbrite crystals, and lowest in the body of the ignimbrite, where some quartz crystals are inclusion-free. Inclusion abundance is dependent on crystal growth rate [*Roedder*, 1984], which is, in turn, dependent on diffusion rate of major structural components in the magma [*Ghiorso*, 1987]. Thus crystals growing in the more H_2O-rich portion of the melt should contain more MI. The average abundance of MI is much lower in feldspar crystals than in quartz crystals for any given sample. This feature, however, probably does not indicate that the feldspar crystals grew in a more volatile-poor magma than did quartz, but rather that the probability of MI entrapment is dependent on crystal type. The regularity of crystal morphology during growth varies with crystal type, and will affect the likelihood of trapping MI. Quartz may grow in a non-faceted morphology [*Kirkpatrick*, 1975] which may promote MI entrapment.

Evidence for Volatile Saturation in the Bandelier Magma

Several lines of evidence suggest that parts of the magma which produced the Bandelier Tuff may have been volatile saturated. The mean water content of the melt phase of the first-erupted Bandelier magma was ~5 wt %. Based on the solubility of water in a rhyolitic melt [*Burnham*, 1975, 1979*a*; *Silver et al.*, 1990], this magma would be water-saturated at depths of 5-6 km. At the present time, this is the best estimate for the depth to the Bandelier magma chamber [*Goff et al.*, 1989].

The covariation of H_2O and F is further evidence for water saturation of the LBT magma. Water and F are both enriched in the magma from the body of the ignimbrite to the base of the ignimbrite to the top of the Plinian tephra. Although there is no

apparent correlation between H_2O and F content of individual MI within samples from the magma which produced the LBT Plinian, the mean H_2O content of samples (averages of multiple MI) increases only slightly, if at all, while mean F increases dramatically. A possible explanation for this behavior is that the upper level of the LBT magma chamber was water-saturated so that the water content of the melt was buffered by the presence of the vapor phase. Any additional H_2O introduced into the melt by crystallization, or other processes, would partition into a vapor phase, leaving the H_2O content of the melt unchanged. However, if F were transported to the upper portion of the magma chamber by the same process as H_2O, it could become enriched in the silicate melt while H_2O remained constant because of the greater compatibility of F in a silicate melt over an H_2O-dominated fluid (fluid/silicate melt partition coefficients are <0.5; *Webster et al.* [1987]; *London et al.* [1988]). This would lead to concentration of F in the evolving magmatic system.

In contrast to F, the mean Cl content of samples from the upper portion of the magma chamber were similar (Tables 3 and 4), and the maximum Cl content of the melt for all samples was virtually identical (Figure 7*b*). Chlorine behaves very much like H_2O, and this behavior is consistent with water saturation because Cl partitions preferentially into an H_2O-rich vapor phase from a rhyolitic melt [*Kilinc and Burnham*, 1972]. The experimentally determined maximum Cl content in water-saturated rhyolites at 2 kbar is 2600 ppm [*Webster and Holloway*, 1988], which is identical to the maximum Cl content of MI from the LBT Plinian eruption. In contrast, Cl contents of MI from the Upper Bandelier (UB) Plinian eruption are uniformly greater than 2600 wt % (Table 3), which, according to the work of *Webster and Holloway* [1988], would only be possible if no H_2O-rich vapor phase were present. *Shinohara et al.* [1989] suggest that the solubility of Cl in a melt is inversely pressure dependent, in which case the higher Cl contents of the UB magma could simply indicate that the UB magma resided higher in the crust than the LBT magma. However, the water content of the UB Plinian suggests that the magma would have been saturated at 3- to 4-km depth, which is shallower than has been estimated for the UB magma chamber [*Goff et al.*, 1989]. However, the Cl content of samples from all parts of the LBT are similar, and the maximum Cl contents of virtually all MI analyzed from the LBT, with the exception of high-Ti MI, are virtually identical. While these data do not negate the above arguments, they show that Cl and H_2O did not behave similarly in the magmatic system as a whole.

Measurements by *London et al.* [1988] and *Pichavant* [1981] suggest high fluid/melt partition coefficients for B of ~2 and ~3 respectively. Assuming that B is partitioned into a hydrous fluid, a plot of F versus B should show similar characteristics to the plots of F versus Cl and F versus H_2O. As Figure 7*c* reveals, this is indeed the case. Thus all identified hygrophilic elements show similar behavior in the MI, with the Plinian samples notable for their high F contents. The behavior of F and H_2O, together with the independent depth estimates, strongly suggests that a hydrous fluid was present in the upper levels of the magma chamber.

DISCUSSION OF TRACE ELEMENT SYSTEMATICS

Trace element compositions of MI from the LBT Tuff are variable, and encompass a similar range of values as observed for pumice lumps, although the major element compositions are invariant (Figures 4*a*-4*f*, Table 2). The range of trace element contents in Plinian MI overlaps with bulk Plinian pumice analyses, as well as with the more trace-element-rich ignimbrite MI compositions. In addition to the normal trend of trace element variation, there is the high-Ti trend described earlier. It does not appear that the observed trace element variations can be explained by a single, simple process. Some processes that may have contributed to the observed variations are discussed here.

Magma Mixing

Trace element compositions of some MI from the LBT ignimbrite appear to show evidence of input of magma that is chemically distinct from "typical" LBT magma that defines the trace element trends described by *Kuentz* [1986]. A group of MI from some pumice lumps have very high Ti and low Nb (Figure 4*e*). Cerium, Ba, Sr, and Zr are high in high-Ti MI, and in contrast, B and Cl are low in these ~20 high-Ti MI (e.g., Figure 4*f*). Populations of low Cl (1000 to 1500 ppm) and B (10-20 ppm) MI, which are all high-Ti MI, can be observed in Figures 7*b* and 7*c*. Major elements appear to be invariant in all MI. The observed variations in MI composition, which cannot be explained by fractional crystallization, suggest that a second magmatic component influenced the composition of part of the Bandelier magma chamber. This type of compositional variation has also been observed in the Bishop Tuff [*Hervig and Dunbar*, 1992; *Dunbar and Hervig*, 1992].

If the second magma was derived from the lower portion of the magma which produced the LBT, eruptions subsequent to the LBT ignimbrite might be expected to show chemical affinities with the second component. This is the case, as evidenced by the first Cerro Toledo tephra erupted after the LBT ignimbrite [*Stix and Gorton*, 1990; J.Stix, personal communication, 1990] which is enriched in Zr (312 ppm), Ti (720 ppm), Ce (124 ppm), Sr (11 ppm) and depleted in Cl (840 ppm) and Nb (50 ppm) as compared to typical LBT magma (Table 5) although their major element compositions are similar. Recent ion microprobe analyses of MI from this tephra confirm that B is also low (9 ppm [*Layne and Stix*, 1990]). These data suggest that the anomalously high-Ti composition of some MI in the LBT ignimbrite may represent a second magma which underlay the "normal" LBT magma.

Introduction of a second magma of similar major element composition but distinct trace element composition into the lower portion of the Bandelier magma chamber may not have affected the crystallizing phase assemblage, but, barring a deviation from Henry's law behavior for trace element partition coefficients, some phenocrysts should record the different trace element composition of the second magma. We measured trace element variations in three sanidine crystals from BB-027, which contains Ti-rich MI derived from the second magma. The results of a step scan on one crystal are shown in Figures 6*a*-6*c*. Note that Ba, Sr, Ti, and Ce are low and constant in the phenocryst core. At about 400 μm from the edge of the phenocryst, these elements all start to increase markedly. Wide variations in trace element composition have been found at the edges of many sanidine crystals from the LBT, but these are especially pronounced. Barium, Sr, Ti, and Ce are strongly correlated in the sanidine, which further suggests that the Ti-rich MI do reflect a dramatic change in the magmatic composition around this phenocryst during crystal growth. Further evidence comes from the presence of two MI in a single phenocryst, one displaying the Ti-rich component, one not (Table 4, BB-004, quartz 4; BB-030 qtz 13). The different rate of increase of elements rimwards probably relates to differences in the diffusion rates of these trace elements sanidine and the mixing silicate magmas [*Hervig and Dunbar*, 1992].

Although the process that we describe here is not large-scale, complete mixing of two strongly different endmembers [e.g.,

Anderson, 1976], it does represent local interaction between two chemically distinct magmas. This interaction is likely to have been place in the lower portion of the magma chamber, because the composition of the second magma is similar to magmas erupted after the LBT. Although the high-Ti magmatic component is most pronounced in the ignimbrite samples with the lowest whole-pumice Nb contents, it can be identified in most ignimbrite samples, but is not found in the Plinian tephra. The presence of this high-Ti, low Nb component, and its apparent influence on the bulk Nb content of ignimbrite pumice samples suggests that some of the apparent syn-eruptive mixing suggested by *Kuentz* [1986] may be due to pre-eruptive inhomogeneities in the magma chamber.

Fractional Crystallization

Although some of the compositional variation observed in MI from the LBT magma can be adequately explained by mixing of a high-Ti, -Ba, -Sr, -Ce rhyolite into the base of the LBT chamber at some time prior to eruption, the dominant compositional variation in the LBT MI and pumice are expressed as the linear correlations between a number of trace elements shown in Figures 4*a* and 4*b*. Liquid compositions below 100 ppm Nb may have been affected by the magma mixing process, but those above 120 ppm probably are not. The close correlation between the pumice and MI compositions suggest that the same evolutionary process affected both. This variation was attributed to fractional crystallization by *Kuentz* [1986]. Fractional crystallization in the body of "normal" LBT magma (not including the high-Ti component) could have produced enrichments of incompatible elements such as Nb, Rb, Y, Th, Ce, and Zr, and could have generated the array of MI compositions observed for those elements. Fractionation of a eutectic assemblage is necessary, because the major element composition of the pumice is invariant. The major mineral phases in the LBT magma are quartz and sanidine, with subordinate pyroxene, and magnetite, and trace amounts of zircon and allanite [*Kuentz*, 1986]. Trace amounts of chevkinite have also been reported [*Izett and Wilcox*, 1968]. As such, the bulk partition coefficients for several trace elements (Rb, Y, Nb, Th, Cl, and F) are $<<1$. The effects of fractional crystallization can be calculated as follows. For Rayleigh fractionation,

$$\frac{x_i^f}{x_i^o} = F^{D_i-1}$$

where x_i^o is the concentration of element i in the initial melt, x_i^f is the concentration of i in the melt after f fraction crystallization, F is fraction of melt remaining ($f=1-F$) and D_i is the crystal/melt partition coefficient for element i. If $D_i=0$, this simplifies to

$$\frac{x_i^f}{x_i^o} = \frac{1}{F}$$

Selection of initial liquid composition. Recognition of magma mixing in the LBT magma is important in order to establish a reasonable starting point for fractional crystallization calculations as these models are profoundly affected by the initial composition selected. In the ideal case, we could use the bulk analysis of the most unevolved pumice lump as the initial composition. Admixing of the distinctive, high-Ti magma, which has altered the bulk magmatic composition, and makes selecting a starting point more difficult. *Kuentz's* [1986] bulk analyses reveal that a change in slope is present on plots of Nb versus Th, Sc, Eu, Zr, Pb, and Ga, at approximately 100 ppm Nb (representative example, Figure 8). Magmatic compositions with <100 ppm Nb may represent magmas containing significant amounts of the high-Ti component (Figure 4*e*). There is a compositional gap between 100 and 120 ppm Nb (Figure 8), so we have chosen 120 ppm Nb as an initial liquid composition, and used the data from *Kuentz* [1986] to determine the concentrations of other elements at this Nb content.

Fractional crystallization modeling of trace elements. The positive linear correlations between Nb and trace elements Th, Y and Rb in Figure 9 might result from fractional crystallization of up to 40% was calculated for phases free of these elements. The observed variation of Nb vs. Zr for MI (Figure 8*a*) could also be a result of 40% fractional crystallization. However, a number of MI contain anomalously high Zr contents. Overlap onto a microcryst of zircon during analysis could be responsible for the high Zr, for even a very small overlap (<0.03 modal percent zircon) could generate the deviant values.

timing of mixing vs fractional

A plot of Nb versus Ce content of MI shows a nearly flat trend with some MI having high Ce contents. This can be explained by the presence of trace amounts of chevkinite in the fractioning assemblage. Analyses of chevkinite in other localities compared

very late

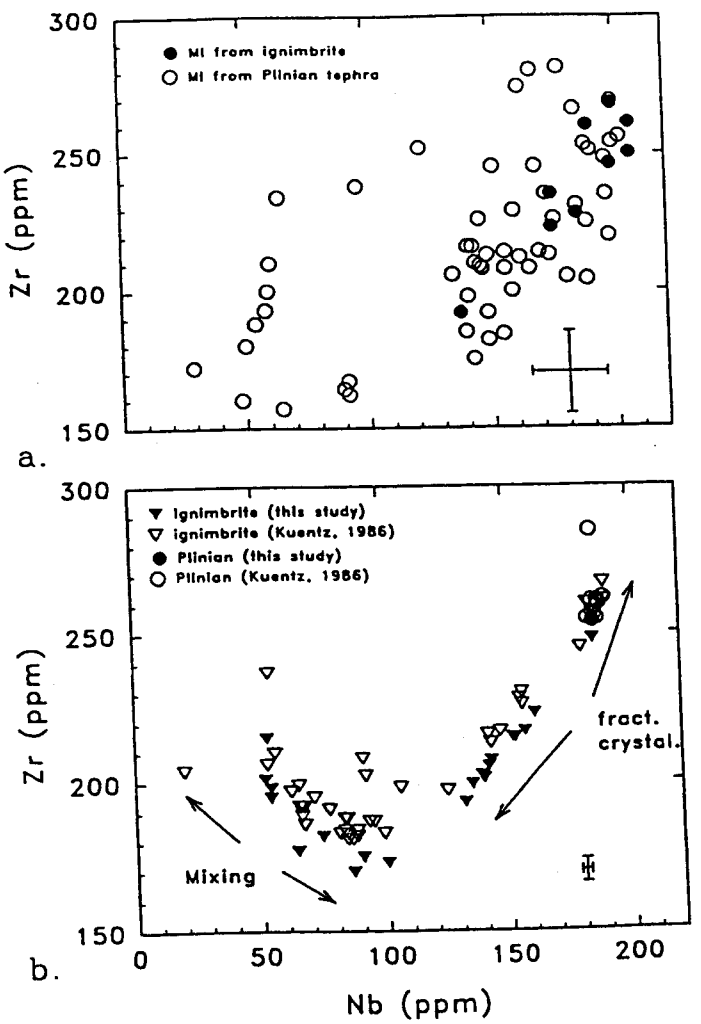

Fig. 8. Plot of Nb versus Zr content for (*a*) melt inclusions and (*b*) pumice lumps from the LBT ignimbrite, and bulk pumice samples from the LBT plinian tephra, as analyzed by Xray fluorescence. Two distinct correlation trends are discernible on plot *b*, one interpreted as magma mixing, the other as possibly a fractional crystallization process.

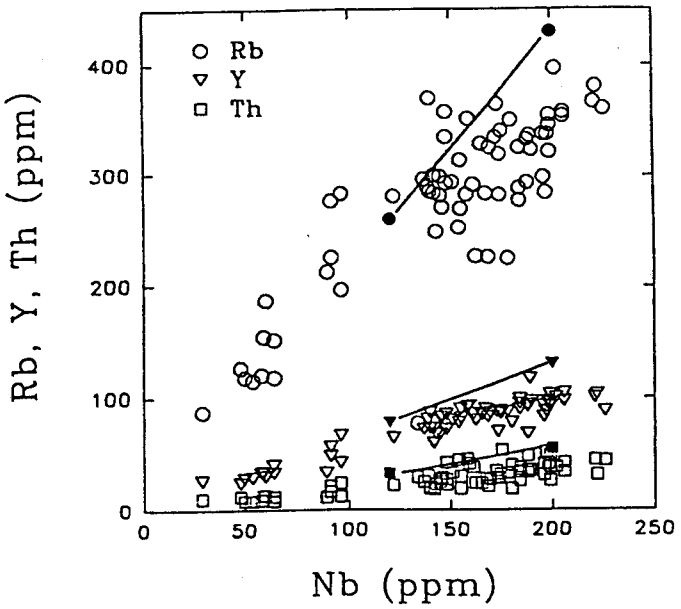

Fig. 9. Calculated fractional crystallization paths and observed compositions for Rb, Th, and Y versus Nb. The solid lines represent from 0 to 40% fractional crystallization, and the open symbols represent the observed melt inclusion compositions. Fractional crystallization calculations are discussed in the text.

to host rocks yields high Ce partition coefficients of 1100-1700 [*Michael*, 1988]. With such a high partition coefficient, fractionation of about 0.1 modal percent chevkinite will yield a bulk partition coefficient near unity, resulting in little variation in Ce in the residual melt during crystallization, with the occasional high Ce resulting from overlap of the ion beam on a microphenocryst of chevkinite.

Other elements. Although is is possible to model evolution of the LBT MI as fractional crystallization with trace elements conventionally used as petrologic indicators, a number of other elements do not seem to fit this model. H_2O, F, Li, and B, which are generally considered to represent the volatile component of a silicate melt, but are also incompatible in the crystallizing phase assemblage, do not exhibit the same trend in MI as nonvolatile trace elements. These are elements which are not normally representatively preserved in bulk rock, and are not generally used as indicators of fractional crystallization. There is a weak positive correlation between Nb and Cl in MI. However, there is no correlation between Nb and F, B, Li or H_2O. If the initial concentration of Cl were 0.15 wt %, slightly over 40% crystallization would be required to explain the Cl contents of the most enriched MI, but the poor correlation makes this conclusion doubtful. Water and F can be considered incompatible in the LBT magma as long as no fluid phase were separating from the melt. The lack of correlation between these components and Nb do not support a model of compositional variation based on fractional crystallization, suggesting that H_2O and F are decoupled from other trace elements in the magmatic system. All may be excluded from the crystalline phases, but H_2O and F may be concentrated upwards by a different mechanism, and/or at a faster rate than the other elements [e.g., *Trial and Spera*, 1990]. However, this explanation cannot be applied to Li and B because of their slower diffusion rates, so their invariance must be due to another process. Both are compatible in an H_2O-rich fluid phase under certain conditions [*Webster et al.*, 1989; *Pichavant*, 1981; *London et al.*, 1988], and could be buffered by such a fluid. However, the low measured H_2O content of the LBT magma precludes presence of an H_2O-rich vapor. A remaining possibility is that these elements were buffered by a CO_2-rich vapor phase, but we have no direct evidence for the presence of CO_2 and no information about the behavior of Li and B in the presence of CO_2-rich vapor.

An alternative explanation for the variation in trace elements, also not without contradictory evidence, is to invoke an additional magma mixing event(s) early in the history of the chamber. While we have abundant evidence for the mixing of a high-Ti rhyolitic component, evidence for an earlier mixing event is mainly supported by the inability of local fractional crystallization to completely explain the chemistry of MI. The only direct evidence for magma mixing lies in the wide range of composition observed in MI from the same crystal host (Table 3). For example, examine Qtz 13 from ignimbrite sample 030. To explain this chemistry would require a strong change in magmatic composition during crystal growth, or simply the mixing of two batches of rhyolite with subtly different trace element composition.

EVOLUTION AND ERUPTION OF THE LOWER BANDELIER TUFF

Although the H_2O and F contents of the LBT magma are variable, and are strongly enriched in the upper portions of the magma chamber, the distribution of these components within the magma chamber is not the same as the distribution of nonvolatile trace elements. The H_2O and F contents of MI from the Plinian tephra are proportionally more strongly enriched than those of lithophile trace elements as compared to ignimbrite compositions. Furthermore, although the nonvolatile trace element compositions of the Plinian and more-enriched ignimbrite MI overlap, the H_2O and F contents of these MI are generally distinct. The net enrichment of non-volatile trace elements can be explained by 40% fractional crystallization, whereas H_2O increases by approximately a factor of 3 from the ignimbrite to the Plinian tephra. The observed variation suggests that the process of concentrating of H_2O and F in the upper part of the magma chamber was more efficient than the process affecting other trace elements. The same pattern is observed for MI from the Bishop Tuff Plinian and ignimbrite deposits [*Hervig and Dunbar*, 1992; *Dunbar and Hervig*, 1992]. Fractional crystallization, particularly sidewall crystallization, has been called on in other systems to explain upward enrichment of incompatible trace elements [*Turner*, 1980] and *Spera et al.* [1989] and *Trial and Spera* [1990] suggest that rapidly diffusing components, particularly H_2O, may become enriched upward much more rapidly than slower-diffusing elements. Prior to the onset of the LBT eruption, an H_2O-rich vapor phase was generated in the upper portion of the magma chamber, as evidenced by the proportionally greater increase in contents of F over H_2O contents of MI, and the invariance of Cl and B in MI from the Plinian tephra. Experimental evidence suggests that Cl and B would fractionate strongly into an H_2O-rich vapor phase [*Kilinc and Burnham*, 1972; *Pichavant*, 1981], so could remain invariant in the melt once a vapor phase had been generated. However, if the vapor phase did not escape the magma chamber after its generation, the magma chamber would have become overpressured [*Burnham*, 1979b, *Tait et al.*, 1989]. An estimate of the overpressure can be determined by comparing the concentration gradients of F and H_2O. Fluorine increases by about 30% from midway through the Plinian (BB-094) to the base of the Plinian tephra (BB-096), whereas increase in H_2O contents is less. Assuming that H_2O was enriched in the magma at the same rate as F, the H_2O content of

No

What

genetic link

What

Why F!

incorrect

up? chemical potential gradients are down? up by gravity

the base of the Plinian would have been ~6.8 wt %, so ~1.5 wt % H_2O has exsolved. Given that the LBT Plinian has a D.R.E. volume of 20 km^3, or a mass of 5.3×10^{16} g, then a total mass of 1×10^{14} g of H_2O would have exsolved from the melt, if the entire Plinian magma was saturated. At a pressure of 2 kb, assuming ideal gas behavior, this mass of H_2O vapor would occupy 1 km^3 in the magma chamber and would generate considerable overpressure. It is likely that as water vapor evolved in the chamber, minor failure in the roof of the magma chamber occurred, as described by *Tait et al.* [1989]. The magma chamber may have behaved as an open system with respect to a vapor component, allowing the vapor to continuously escape as it was generated. Geothermal fluids related to magmatic systems, and in some cases, gas content of soils around active volcanoes, contain a magmatic component, suggesting that magmas are able to degas passively [e.g., *Burnham*, 1979b; *Allard et al.*, 1989]. Assuming that excess volatile components were able to escape from the chamber, the eruption of the LBT was probably not caused by simple, progressive buildup of volatile components in the upper portion of the chamber, but may have instead been initiated by a more catastrophic event, such as influx of new magma, or tectonic disturbance [*Sparks et al.*, 1977].

The LBT eruption appears to have been characterized by removal and deposition of discrete horizons of the magma chamber, followed by chaotic eruption of deeper magma [*Kuentz*, 1986]. The density and viscosity variations in a magma chamber strongly influence the withdrawal mechanisms of the magma from the chamber, and can, in turn, strongly affect the eruptive style [*Blake*, 1984; *Blake and Ivey*, 1986; *Spera et al.*, 1986]. Based on the volatile and major element compositions of the LBT Plinian and ignimbrite magmas, density and viscosity variations within the magma chamber have been estimated (Figure 10) in order to relate these changes to the eruptive style. The density of the magma was calculated for a temperature of 850°C (based on estimates of Upper Bandelier Ignimbrite magma from *Warshaw and Smith* [1988] using partial molar volumes from *Mo et al.* [1982] and *Burnham and Davies* [1971]). The partial molar volumes for all components except H_2O were determined for a pressure of 1 bar, as data are not currently available to determine the absolute density of the magma at 2 kbar. However, the objective of these calculations is to determine the density difference between the water-rich and water-poor LBT magma, and if this difference for the LBT magma is analogous to albitic melts studied by *Burnham and Davies* [1971], the variable H_2O content of the magma has a much stronger effect on the calculated magmatic density than the compressibility of anhydrous components, or that of reasonable variations in temperature. The viscosity was calculated following the method of *Shaw* [1972]. The effect of F on melt viscosity is roughly similar to that of water [*Dingwell*, 1987] and for viscosity calculations of the Bandelier magma, the F content of the melt was added to that of water. Magmatic phenocryst content was not included in the calculations because the phenocryst content is generally low (<20% corrected for vesicularity) and there is no evidence of strong systematic variations in phenocryst content throughout the Bandelier magma [*Kuentz*, 1986].

The density and viscosity of the Bandelier magma are strongly affected by magmatic water content, therefore the largest change in these magmatic properties per volume of magma occurred within the upper part of the chamber (see Figure 10). The magma which produced the bulk of the Plinian tephra appears to have been saturated with H_2O, which could have drastically reduced the bulk density. The body of the ignimbrite was relatively homogeneous with respect to water, and therefore, assuming that no CO_2-rich vapor phase was present, with respect to magmatic density and viscosity as well.

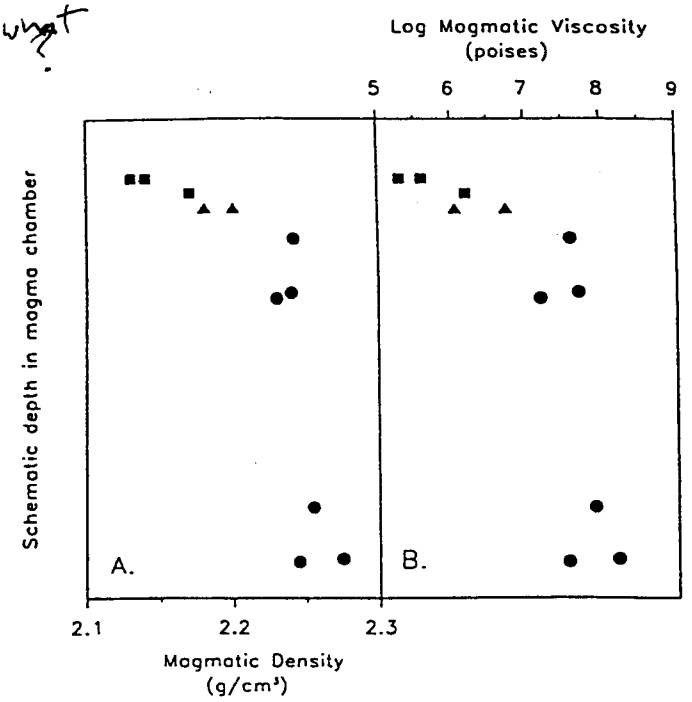

Fig. 10. Calculated magmatic (*a*) density and (*b*) viscosity versus inferred depth in the LBT magma chamber. The depth in the chamber is roughly based on the volume of erupted material for the plinian and the basal ignimbrite, and is inferred based on the Nb content of the sample for the body of the ignimbrite. Mean H_2O contents of MI are used for each sample, and a temperature of 850°C is used throughout.

The non-uniform density and viscosity variations within the Bandelier magma may have influenced the eruption dynamics of the magma, causing withdrawal of discrete compositional layers of magma in the early stages of the eruption, followed by the more chaotic style of eruption which may characterize the body of the ignimbrite, in which a number of compositional layers were tapped simultaneously, and mixed. This behavior is consistent with the eruptive styles predicted for magmas as a function of density and viscosity gradients [*Blake and Ivey*, 1986; *Spera*, 1984; *Spera et al.*, 1986]. However, as discussed in *Dunbar and Hervig* [1992] the magma which produced the Bishop Tuff appears to have contained a similar volatile gradient to the Bandelier magma, although the eruptive style of the Bishop ignimbrite appears to be more regular than that of the LBT ignimbrite. Furthermore, the H_2O content of the magma at the Plinian:ignimbrite transition of these two eruptions is quite different; 4.3 wt % for the LBT and 2.6 wt % for the Bishop Tuff. As vent width is one of the factors which controls Plinian versus ignimbrite eruptive style [e.g., *Wilson et al.*, 1980], a possible reason for this difference is that the vent of the LBT eruption may have widened drastically after 20 km^3 of magma was erupted, precipitating the onset of ignimbrite eruption. A catastrophic vent widening, perhaps associated with caldera collapse, could have disrupted the eruption style to the point where chaotic, rather than systematic, withdrawal occurred. The above observations suggest that although the volatile components of a magma are the driving force behind explosive volcanic eruptions, the volatile gradient of a magmatic system is not necessarily the primary factor controlling the eruption dynamics, and that other factors, such as the geometry of the magma chamber and vent systems, may also be important.

critical Rayleigh # $Ra = \frac{\rho_0 g \alpha \Delta T b^3}{\eta \kappa}$ b = distance, η = viscosity, κ = thermal diffusivity, α = coeff. thermal expansion

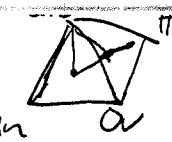

The LBT eruption ended after approximately 400 km^3 of magma had been erupted, but the volatile content of the magma did not decrease markedly towards the end of the eruption. However, tapping of the high-Ti magma underlying the normal LBT magma may have caused the LBT eruption to end. The reason for termination, however, is not immediately clear, because although the Cl content of the Ti-rich magma is low, the water content, major element concentrations, and crystallinity do not appear notably different than the LBT magma. Melt inclusions in the tephra directly overlying the LBT ignimbrite contain 2.5 wt % H_2O [*Layne and Stix*, 1990], further suggesting that the high-Ti and LBT magmas contained similar H_2O contents. Possible reasons for eruption termination, such as a sudden change in magmatic density, or decrease in vesiculation behavior, are not supported by the observed compositional similarity. Other physical properties of the high Ti magma, or the interface between the dominantly high and dominantly low Ti magmas not apparent from our analyses, may have caused the eruption to cease, or the eruption could have been terminated by further caldera collapse.

CONCLUSIONS

1. Analysis of melt inclusions from the Lower Bandelier Plinian tephra and ignimbrite indicate that a volatile gradient was present in the pre-eruptive magma. Magmatic H_2O and F range from around 5.5 to 1.5 wt %, and from 3500 to 500, ppm respectively, from the base of the Plinian to the top of the ignimbrite. The volatile gradient was strongest in the magma that produced the Plinian tephra and the basal ignimbrite, and was much less pronounced in the magma that formed the body of the ignimbrite. Variation in the magmatic volatile content appears to have been decoupled from trace element variations observed in whole-pumice analyses and in MI.

OK.

2. The upper portion of the LBT magma chamber appears to have been saturated with respect to a H_2O-rich volatile phase, as evidenced by a continuous increase in magmatic F contents with no corresponding increase in magmatic H_2O. Elements Cl and B apparently partitioned into the vapor phase, as would be expected from experimentally determined partition coefficients.

why?

3. The initial part of the LBT eruption removed relatively discrete compositional layers of magma, consistent with a magma with a strong density and viscosity gradient, whereas during eruption of the main body of the ignimbrite, different portions of the magma chamber were tapped concurrently. The volatile gradient of the LBT is qualitatively similar to that of the Bishop Tuff, which was apparently erupted sequentially from a zoned chamber. The H_2O content of the initially-erupted ignimbrite samples is higher for the LBT than for the BT. This suggests that eruption dynamics is, in large part dependent on vent configuration, and that relatively early caldera collapse may have affected eruption of the LBT.

Nope

4. Magmatic volatile contents of the Upper Bandelier Plinian tephra were subtly different from those of the Lower Bandelier Plinian. The UB magma may not have been saturated with respect to a volatile phase at the time of eruption. The Bandelier magmatic system was able to regenerate to near its original composition in the 300,000 yrs between these two eruptions.

5. Part of the compositional variation in the LBT, as observed in both whole pumice samples and MI, could have been generated by 40% fractional crystallization. However, the lack of correlation between H_2O, F, and other trace elements, along with the high degree of enrichment of H_2O and F in the upper region of the magma chamber, suggests that these components were highly mobile in the magmatic system, and were able to move upwards at a faster rate than other trace elements.

6. Evidence for magma mixing is observed in some MI compositions from the top of the LBT ignimbrite. These MI have compositions that can be explained by up to a 50% mixture between the LBT magma and a compositionally distinct, high-Ti rhyolitic magma which erupted from the Valles caldera following the LBT. Removing the late-stage, high-Ti component has a profound impact on models of fractional crystallization, and shows that the trace element composition of the LBT magma chamber was less variable than previously thought. As much as any other conclusion, this emphasizes the utility of microbeam trace element analysis in its ability to detect compositional variations that may be overlooked by bulk analytical techniques. Other large eruptions should be investigated in order to determine if apparent compositional gradients are partly due to mixing events.

Acknowledgements. Thanks go to a number of people who have contributed to various aspects of this research. We would particularly like to thank J. Clark for assistance with the electron microprobe; B. Thomas for assistance with the ion microprobe; S. Balsley and W. McIntosh for guidance and assistance in the field; H. Sigurdsson, E. Stolper, and H. Westrich for providing ion microprobe standards; P. Kyle and W. McIntosh for informal reviews and discussion; and F. Anderson for useful discussion and for steering us in the direction of fractional crystallization. Thanks to C. Bacon and S. Blake for constructive and insightful reviews. The electron microprobe was purchased with the aid of NSF grant EAR-8408163 (to P. Buseck). This research was supported by NSF grant EAR-8803694 (to NWD) and EAR-88-14652 (to RLH).

REFERENCES

Allard, P., J. C. Baubron, J. Carbonnell, D. Dajlevic, J. LeBronec, M. C. Robe, P. Zettwoog, and J. D. Toutain, Diffuse soil degassing from volcanoes: geochemical and volcanological implications, *N. M. Bur. Mines Min. Resour. Bull.*, *131*, 3, 1989.

Anderson, A. T., Magma mixing: petrological processes and volcanological tool, *J. Volcanol. Geotherm. Res.*, *1*, 3-33, 1976.

Anderson, A. T., Hourglass inclusions: Theory and application to the Bishop Rhyolite Tuff, *Am. Mineral.*, *76*, 530-547, 1991.

Anderson, A. T., and T. L. Wright, Phenocrysts and glass inclusions and their bearing on oxidation and mixing of basaltic magmas, Kilauea Volcano, Hawaii, *Am. Mineral.*, *57*, 188-216, 1972.

Bacon, C. R., Eruptive history of Mount Mazama and Crater Lake caldera, Cascade Range, U.S.A, *J. Volcanol. Geotherm. Res.*, *18*, 57-118, 1983.

Bacon, C. R., Crystallization of accessory phases in magmas by local saturation adjacent to phenocrysts, *Geochim. Cosmochim. Acta*, *53*, 1055-1066, 1989.

Bacon, C. R., S. Newman, and E. Stolper, Water, CO_2, Cl, and F in melt inclusions in phenocrysts from three Holocene explosive eruptions, Crater Lake, Oregon, *Am. Mineral.*, in press, 1992.

Balsley, S. D., The petrology and geochemistry of the Tshirege member of the Bandelier Tuff, Jemez Mountains volcanic field, New Mexico, USA, M.S. thesis, Univ. of Tex., Arlington, 1988.

Belkin, H. E., B. De Vivo, E. Roedder, and M. Cortini, Fluid inclusion geobarometry from ejected Mt. Somma-Vesuvius nodules, *Am. Mineral.*, *70*, 288-303, 1985.

Blake, S., Volatile oversaturation during the evolution of silicic magma chambers as an eruption trigger, *J. Geophys. Res.*, *89*, 8237-8244, 1984.

Blake, S., and I. H. Campbell, The dynamics of magma-mixing during flow in volcanic conduits, *Contrib. Mineral. Petrol.*, *94*, 72-81, 1986.

Blake, S., and G. N. Ivey, Magma-mixing and the dynamics of withdrawal from stratified reservoirs, *J. Volcanol. Geotherm. Res.*, *27*, 153-178, 1986.

Burnham, C. W., Water and magma: a mixing model, *Geochim. Cosmochim. Acta*, *39*, 1077-1084, 1975.

Burnham, C. W., Importance of volatile constituents, in *Evolution of Igneous Rocks, Fiftieth Anniversary Perspectives*, edited by H. D. Yoder, pp. 439-482, Princeton University Press, Princeton, N.J. 1979*a*.

Burnham, C. W., Magmas and hydrothermal fluids, in *Geochemistry of Hydrothermal Ore Deposits*, 1st ed., edited by H. L. Barnes, pp. 71-133. John Wiley, New York, 1979b.

Burnham, C. W., and N. F. Davies, The role of H_2O in silicate melts, I, P-V-T relations in the system $NaAlSi_3O_8$-H_2O to 10 kilobars and 1000°C, *Am. J. Sci.*, *270*, 54-79, 1971.

Carrigan, C. R., and J. C. Eichelberger, Zoning of magmas by viscosity in volcanic conduits, *Nature*, *343*, 248-251, 1990.

Devine, J. D., H. Sigurdsson, and A. N. Davis, Estimates of sulfur and chlorine yield to the atmosphere from volcanic eruptions and potential climatic effects, *J. Geophys. Res.*, *89*, 6309-6325, 1984.

Dingwell, D. B., Melt viscosities in the system $NaAlSi_3O_8$-H_2O-F_2O_{-1}, in *Magmatic Processes: Physiochemical Principles, Spec. Publ. 1*, edited by B. O. Mysen, pp. 423-431, Geochemical Society, University Park, PA, 1987.

Dunbar, N. W., Lack of volatile gradient in the Taupo plinian-ignimbrite eruptive transition: Evidence from melt inclusion analysis, *EOS, Trans. AGU*, *72*, 569, 1991.

Dunbar, N. W., and R. L. Hervig, Volatile and trace element composition of melt inclusions from the Lower Bandelier Tuff: Implications for eruptive style and magma chamber processes, *J. Geophys. Res.*, in press 1992.

Dunbar, N. W., R. L. Hervig, and P. R. Kyle, Determination of pre-eruptive H_2O, F and Cl contents of silicic magmas using melt inclusions: Examples from Taupo volcanic center, New Zealand, *Bull. Volcanol.*, *51*, 177-184, 1989*a*.

Dunbar, N. W., P. R. Kyle, and C. J. N. Wilson, Evidence for limited zonation in silicic magma systems, Taupo Volcanic Zone, New Zealand, *Geology*, *17*, 234-236, 1989*b*.

Ghiorso, M. S., Chemical mass transfer in magmatic processes, *Contrib. Mineral. Petrol.*, *96*, 291-313, 1987.

Goff, F., J. N. Gardner, W. S. Baldridge, J. B. Hulen, D. L. Nielsen, D. Vaniman, G. Heiken, M. A. Dungan, and D. Broxton, Volcanic and hydrothermal evolution of pleistocene Valles Caldera and Jemez Volcanic Field, *N.M. Bur. Mining Min. Res. Mem.*, *46*, 381-431, 1989.

Hervig, R. L., and N. W. Dunbar, Cause of chemical zoning in the Bishop and Bandelier magma chambers, *Earth Planet. Sci. Lett.*, *111*, 97-108, 1992.

Hervig, R. L., and P. Williams, SIMS microanalysis of minerals and glasses for H and D, in *Secondary Mass Spectrometry, SIMS VI*, edited by A. Benninghoven, A. M. Huber, and H. W. Werner, pp. 961-964, John Wiley, New York, 1988.

Hervig, R. L., T. T. Stanton, and P. Williams, Ion Probe microanalysis of hydrogen in glasses and minerals, *EOS, Trans. AGU*, *68*, 441, 1987.

Hervig, R. L., Dunbar, N. W., Westrich, H. R., and P. R. Kyle, Pre-eruptive water content of rhyolitic magmas as determined by ion microprobe analyses of melt inclusions in phenocrysts, *J. Volcanol. Geotherm. Res.*, *36*, 293-302, 1989.

Hildreth, W., The Bishop Tuff: Evidence for the origin of compositional zonation in silicic magma chambers, *Geol. Soc. Am. Spec. Pap.*, *180*, 43-85, 1979.

Hildreth, W., Gradients in silicic magma chambers: Implications for lithospheric magmatism, *J. Geophys. Res.*, *86*, 10,153-10,192, 1981.

Hofmann, A. W., Diffusion in natural silicate melts: A critical review, in *Physics of Magmatic Processes*, edited by R. B. Hargraves, pp. 385-419, Princeton University Press, Princeton, 1980.

Izett, G. A., and R. E. Wilcox, Perrierite, chevkinite, and allanite in upper cenozoic ash beds in the western United States, *Am. Mineral.*, *53*, 1558-1567, 1968.

Karsten, J. L., J. R. Holloway, and J. R. Delaney, Ion microprobe studies of water in silicate melts: Temperature -dependent water diffusion in obsidian, *Earth Planet. Sci. Lett.*, *59*, 420-428, 1982.

Kilinc, I. A., and C. W. Burnham, Partitioning of chloride between a silicate melt and coexisting aqueous phase from 2 to 8 kilobars, *Econ. Geol.*, *67*, 231-235, 1972.

Kirkpatrick, R. J., Crystal growth from the melt: A review, *Am. Mineral.*, *60*, 798-814, 1975.

Kovalenko, V. I., R. L. Hervig, and M. F. Sheridan, Ion-microprobe analyses of trace elements in anorthoclase, hedenbergite, aenigmatite, quartz, apatite and glass in pantellerite: Evidence for high water contents in pantellerite melt, *Am. Mineral.*, *73*, 1038-1045, 1988.

Kuentz, D. A., The Otowi member of the Bandelier Tuff: A study of the petrology, petrography, and geochemistry of an explosive silicic eruption, Jemez Mountains, New Mexico, M.S. thesis, Univ. of Tex. at Arlington, 1986.

Layne, G. D., and J. Stix, Volatile and light lithophile element evolution of the Cerro Toledo rhyolite, Jemez Mountains, New Mexico: an ion microprobe study, *Eos Trans. AGU*, *76*, 651, 1990.

London, D., R. L. Hervig, and G. B. Morgan, Melt-vapor solubilities and elemental partitioning in peraluminous granite-pegmatite systems: experimental results with Macusani glass at 200 MPa, *Contrib. Mineral. Petrol.*, *99*, 360-373, 1988.

Michael, P. J., Partition coefficients for rare-earth elements in mafic minerals of high silica rhyolites: The importance of accessory mineral inclusions, *Geochim. Cosmochim. Acta*, *52*, 275-282, 1988.

Miller, C. F., and D. W. Mittlefehldt, Extreme fractionation in felsic magma chambers: A product of liquid-state diffusion or fractional crystallization?, *Earth Planet. Sci. Lett.*, *68*, 151-158, 1984.

Mo, X., I. S. E. Carmichael, M. Rivers, and J. Stebbins, The partial molar volume of Fe_2O_3 in multicomponent silicate liquids and the pressure dependence of oxygen fugacity in magmas, *Mineral. Mag.*, *45*, 237-245, 1982.

Nash, W. P., and H. R. Crecraft, Partition coefficients for trace elements in silicic magmas, *Geochim. Cosmochim. Acta*, *49*, 2309-2322, 1985.

Norrish, K., and B. W. Chappell, X-ray fluorescence spectrometry, in *Physical Methods in Determinative Mineralogy*, edited by J. Zussman, pp. 210-272, Academic Press, San Diego, Calif., 1977.

Oldenburg, C. M., F. Spera, D. A. Yuen, and G. Sewell, Dynamic mixing in magma bodies: Theory, simulations, and implications, *J. Geophys. Res.*, *94*, 9215-9236, 1989.

Pichavant, M., An experimental study of the effect of boron on a water saturated haplogranite at 1 kbar vapour pressure, *Contrib. Mineral. Petrol.*, *76*, 430-439, 1981.

Qin, Z., and A. T. Anderson, Experimental reequilibration of a melt inclusion in quartz from a rhyolite: Diffusive loss of water?, *EOS, Trans. AGU*, *73*, 367, 1992.

Roedder, E., *Fluid Inclusions, Reviews in Mineralogy*, 1st ed., vol. 12, Mineralogical Society of America, Washington, DC, 1984.

Self, S., and P. W. Lipman, Large ignimbrites and caldera-forming eruptions- Workshop handbook, IAVCEI Working Group on Explosive Volcanism and Its Products, Field Workshop 11WA, IAVCEI, Santa Fe, N.M., June 15-24, 1989.

Self, S., F. Goff, J. N. Gardner, J. V. Wright, and W. M. Kite, Explosive rhyolitic volcanism in the Jemez Mountains: Vent locations, caldera development and relation to regional structure, *J. Geophys. Res.*, *91*, 1779-1798, 1986.

Shaw, H. R., Viscosity of magmatic silicate liquids: An empirical method of prediction, *Am. J. Sci.*, *272*, 870-893, 1972.

Shinohara, H., J. T. Ilyama, and S. Matsuo, Partition of chlorine compounds between silicate melt and hydrothermal solutions: I. Partitioning of NaCl-KCl, *Geochim. Cosmochim. Acta*, *53*, 2617-2630, 1989.

Silver, L. A., P. D. Ihinger, and E. Stolper, The influence of bulk composition on the speciation of water in silicate glasses, *Contrib. Mineral. Petrol.*, *104*, 142-162, 1990.

Skirius, C. M., J. W. Peterson, and A. T. Anderson, Homogenizing rhyolitic glass inclusions from the Bishop Tuff, *Am. Mineral.*, *75*, 1381-1398, 1990.

Smith, R. L., Ash-flow magmatism, *Geol. Soc. Am. Spec. Pap.*, *180*, 5-27, 1979.

Smith, R. L., and R. A. Bailey, The Bandelier Tuff: A study of ash-flow eruption cycles from zoned magma chambers, *Bull. Volcanol.*, *29*, 83-104, 1966.

Smith, R. L., R. A. Bailey, and C. S. Ross, Structural evolution of the Valles caldera, New Mexico, and its bearing on the emplacement of ring dikes, *U.S. Geol. Surv. Prof. Pap.*, *424-D*, D145-D149, 1961.

Sommer, M. A., and L. S. Schramm, An analysis of the water concentrations in silicate melt inclusions in quartz phenocrysts from the Bandelier Tuff, Jemez Mountains, New Mexico, *Bull. Volcanol.*, *46*, 299-320, 1983.

Sparks, R. S. J., H. Sigurdsson, and L. Wilson, Magma mixing: a mechanism for triggering acid explosive eruptions, *Nature*, *267*, 315-318, 1977.

Spell, T. L., M. T. Harrison, and J. A. Wolff, $^{40}Ar/^{39}Ar$ dating of the Bandelier Tuff and San Diego Canyon ignimbrites, Jemez Mountains, New Mexico: temporal constraints on magmatic evolution, *J. Volcanol. Geotherm. Res.*, *43*, 175-193, 1990.

Spera, F. J., Some numerical experiments on the withdrawal of magma from crustal reservoirs, *J. Geophys. Res.*, *89*, 8222-8236, 1984.

Spera, F. J., D. A. Yuen, J. C. Greer, and G. Sewell, Dynamics of magma withdrawal from stratified magma chambers, *Geology*, *14*, 723-726, 1986.

Stix, J., and M. P. Gorton, Variations in trace element partition coefficients in sanidine in the Cerro Toledo Rhyolite, Jemez Mountains, New Mexico: Effects of composition, temperature, and volatiles, *Geochim. Cosmochim. Acta*, *54*, 2697-2708, 1990.

Stix, J., F. Goff, M. P. Gorton, G. Heiken, and S. R. Garcia, Restoration of compostional zonation in the Bandelier silicic magma chamber between two caldera-forming eruptions: Geochemistry and origin of the Cerro Toledo rhyolite, Jemez Mountains, New Mexico, *J. Geophys. Res.*, *93*, 6129-6147, 1988.

Tait, S., C. Jaupart, and S. Vergniolle, Pressure, gas content and eruption

periodicity of a shallow, crystallizing magma chamber, *Earth Planet. Sci. Lett.*, *92*, 107-123, 1989.

Trial, A. F., and F. J. Spera, Mechanisms for the generation of compositional heterogeneities in magma chambers, *Geol. Soc. Am. Bull.*, *102*, 353-367, 1990.

Turbeville, B. N., and S. Self, San Diego Canyon ignimbrites: Pre-Bandelier Tuff explosive rhyolitic volcanism in the Jemez Mountains, New Mexico, *J. Geophys. Res.*, *93*, 6148-6156, 1988.

Warshaw, C. M., and R. L. Smith, Pyroxene and fayalites in the Bandelier Tuff, New Mexico: temperatures and comparisons with other rhyolites, *Am. Mineral.*, *73*, 1025-1037, 1988.

Watson, E. B., Glass inclusions as samples of early magmatic liquid: Determinative method and application to a South Atlantic basalt, *J. Volcanol. Geotherm. Res.*, *1*, 73-84, 1976.

Webster, J. D., and W. A. Duffield, Preeruptive volatile contents of rhyolitic magma, Taylor Creek, New Mexico, U.S.A.: Variable and extreme F and Cl enrichments, *EOS, Trans. AGU*, *71*, 651, 1990.

Webster, J. D., and J. R. Holloway, Experimental constraints on the partitioning of Cl between topaz rhyolites and H_2O and H_2O+CO_2 fluids: New implications for granitic differentiation and ore deposition, *Geochim. Cosmochim. Acta*, *52*, 2091-2105, 1988.

Webster, J. D., J. R. Holloway, and R. L. Hervig, Phase equilibria and volatile partitioning in a Be, U, and F-enriched vitrophyre from Spor Mountain, Utah, *Geochim. Cosmochim. Acta*, *51*, 389-402, 1987.

Webster, J. D., J. R. Holloway, and R. L. Hervig, Partitioning of lithophile trace elements between H_2O and H_2O+CO_2 fluids and topaz rhyolitic melt, *Econ. Geol.*, *84*, 116-134, 1989.

Wilson, L., R. S. J. Sparks, and G. P. L. Walker, Explosive volcanic eruptions, IV, The control of magma properties and conduit geometry on eruption column behavior, *Geophys. J. R. Astron. Soc.*, *63*, 117-148, 1980.

N. W. Dunbar, Geoscience Department, New Mexico Institute of Mining and Technology, Socorro, NM 87801.

R. L. Hervig, Center for Solid State Science, Arizona State University, Tempe, AZ 85287-1704.

(Received October 22, 1991;
revised June 5, 1992;
accepted June 6, 1992.)